Elevations of intracellular calcium reflect normal voltage-dependent behavior, and not constitutive activity, of voltage-dependent calcium channels in gastrointestinal and vascular smooth muscle

John G. McCarron,[1] Marnie L. Olson,[1] Susan Currie,[1] Amanda J. Wright,[2] Kurt I. Anderson,[3] and John M. Girkin[2]

[1]Strathclyde Institute of Pharmacy and Biomedical Sciences, and [2]Institute of Photonics, SUPA, University of Strathclyde, Glasgow G4 0NR, Scotland, UK

[3]Beatson Institute for Cancer Research, Glasgow G61 1BD, Scotland, UK

In smooth muscle, the gating of dihydropyridine-sensitive Ca^{2+} channels may either be stochastic and voltage dependent or coordinated among channels and constitutively active. Each form of gating has been proposed to be largely responsible for Ca^{2+} influx and determining the bulk average cytoplasmic Ca^{2+} concentration. Here, the contribution of voltage-dependent and constitutively active channel behavior to Ca^{2+} signaling has been studied in voltage-clamped single vascular and gastrointestinal smooth muscle cells using wide-field epifluorescence with near simultaneous total internal reflection fluorescence microscopy. Depolarization (−70 to +10 mV) activated a dihydropyridine-sensitive voltage-dependent Ca^{2+} current (I_{Ca}) and evoked a rise in $[Ca^{2+}]$ in each of the subplasma membrane space and bulk cytoplasm. In various regions of the bulk cytoplasm the $[Ca^{2+}]$ increase ($[Ca^{2+}]_c$) was approximately uniform, whereas that of the subplasma membrane space ($[Ca^{2+}]_{PM}$) had a wide range of amplitudes and time courses. The variations that occurred in the subplasma membrane space presumably reflected an uneven distribution of active Ca^{2+} channels (clusters) across the sarcolemma, and their activation appeared consistent with normal voltage-dependent behavior. Indeed, in the present study, dihydropyridine-sensitive Ca^{2+} channels were not normally constitutively active. The repetitive localized $[Ca^{2+}]_{PM}$ rises ("persistent Ca^{2+} sparklets") that characterize constitutively active channels were observed rarely (2 of 306 cells). Neither did dihydropyridine-sensitive constitutively active Ca^{2+} channels regulate the bulk average $[Ca^{2+}]_c$. A dihydropyridine blocker of Ca^{2+} channels, nimodipine, which blocked I_{Ca} and accompanying $[Ca^{2+}]_c$ rise, reduced neither the resting bulk average $[Ca^{2+}]_c$ (at −70 mV) nor the rise in $[Ca^{2+}]_c$, which accompanied an increased electrochemical driving force on the ion by hyperpolarization (−130 mV). Activation of protein kinase C with indolactam-V did not induce constitutive channel activity. Thus, although voltage-dependent Ca^{2+} channels appear clustered in certain regions of the plasma membrane, constitutive activity is unlikely to play a major role in $[Ca^{2+}]_c$ regulation. The stochastic, voltage-dependent activity of the channel provides the major mechanism to generate rises in $[Ca^{2+}]$.

The Journal of General Physiology

INTRODUCTION

In smooth muscle, Ca^{2+}, which enters from outside the cell across the plasma membrane, controls almost every activity the cell performs, including cell division, growth, contraction, and cell death. Ca^{2+} may control multiple functions because of the cell's ability to create complex spatiotemporal signals by generating local concentrations of Ca^{2+} in certain regions that differ from the cytoplasmic average value (McCarron et al., 2006; Rizzuto and Pozzan, 2006). Different spatiotemporal Ca^{2+} signals evoke various cellular responses. Of the Ca^{2+} entry pathways that exist in smooth muscle, the dihydropyridine-sensitive L-type voltage-dependent Ca^{2+} channel is expressed widely and may dominate in the control of Ca^{2+} entry (Nelson et al., 1990; Gollasch and Nelson, 1997; Sanders, 2008).

Several features of the L-type voltage-dependent channel combine to regulate the flow of Ca^{2+} across the membrane and generate complex spatiotemporal signals. For example, changes in membrane potential (depolarization or hyperpolarization) alter Ca^{2+} influx in a complex way because of its dual influence on channel opening and the electrochemical gradient that generates the flow of Ca^{2+} across the plasma membrane. Depolarization increases and hyperpolarization decreases channel opening (Nelson et al., 1990; Vivaudou et al., 1991; Quayle et al., 1993; Bayguinov et al., 2007) to increase and decrease Ca^{2+} entry, respectively. In response to changes in membrane potential, the opening of the

Correspondence to J.G. McCarron: john.mccarron@strath.ac.uk

J.M. Girkin's present address is Centre for Advanced Instrumentation, Dept. of Physics, Durham University, Durham DH1 3LE, England, UK.

Abbreviations used in this paper: MEL, murine erythroleukemia; TIRF, total internal reflection fluorescence microscopy.

© 2009 McCarron et al. This article is distributed under the terms of an Attribution–Noncommercial–Share Alike–No Mirror Sites license for the first six months after the publication date (see http://www.jgp.org/misc/terms.shtml). After six months it is available under a Creative Commons License (Attribution–Noncommercial–Share Alike 3.0 Unported license, as described at http://creativecommons.org/licenses/by-nc-sa/3.0/).

The Rockefeller University Press $30.00
J. Gen. Physiol. Vol. 133 No. 4 439–457
www.jgp.org/cgi/doi/10.1085/jgp.200810189

channel is usually considered to be a random, stochastic process (Sakmann and Neher, 1995), which seems well suited to the delivery of local transient increases in $[Ca^{2+}]$ to generate complex signals.

The magnitude of flow of Ca^{2+} across the plasma membrane, via an open channel, varies during activation to contribute to the complexity of the Ca^{2+} signal. The magnitude is determined by the open-channel conductance and electrochemical driving force that act on the ion. The latter may vary substantially during normal physiological activation to alter the flux of Ca^{2+} into the cell. The electrochemical driving force, a combination of the Ca^{2+} concentration gradient and the electrical potential across the membrane, is the difference between the Ca^{2+} equilibrium potential and plasma membrane potential. A 30-mV change in membrane potential, well within the normal physiological variation, will produce a change in electrochemical driving force equivalent to a 10-fold change in extracellular Ca^{2+} concentration. Hyperpolarization increases and depolarization decreases the electrochemical driving force to increase and decrease Ca^{2+} entry, respectively.

During physiological activation, the substantial decrease in electrochemical gradient for Ca^{2+} entry that accompanies depolarization is offset by a significantly increased open probability of the channel so that increased Ca^{2+} entry occurs. On the other hand, the increase in Ca^{2+} entry that accompanies hyperpolarization is offset by the reduced open probability of the channels so that the combined effect of hyperpolarization on open probability and driving force is a reduced overall flow of Ca^{2+} into the cell. Clearly, a channel that is persistently open will have a significantly diminished contribution to Ca^{2+} entry as the cell is depolarized as the flux of the ion decreases with driving force.

Another feature that determines the magnitude of Ca^{2+} entry is the density and distribution of the channels. The average density of the L-type voltage-dependent Ca^{2+} channel in smooth muscle is 5–10 per μm^2 (Rubart et al., 1996). In some cell types, voltage-dependent Ca^{2+} channels are not distributed uniformly but clustered in certain regions of the plasma membrane. For example, L-type voltage-dependent Ca^{2+} channels were arranged into around 20 clusters on the basolateral membrane of frog hair cells (Roberts et al., 1990) to produce localized rises in $[Ca^{2+}]_c$ at these sites. The behavior of these clustered channels remained under the control of membrane potential to open and close stochastically; channels were closed at negative membrane potentials and opened with depolarization. N-type Ca^{2+} channels in *Xenopus* oocytes show a patchy distribution in certain regions of the plasma membrane (Demuro and Parker, 2004). Substantial variation in open probability occurred among channels, even those that were adjacent; i.e., the activity of one channel did not appear to influence that of its neighbor; channel gating was stochastic (Demuro and Parker, 2004).

Recently, in smooth muscle, L-type voltage-dependent Ca^{2+} channels have also been proposed to function as clusters in certain regions of the sarcolemma to generate localized Ca^{2+} increases (Navedo et al., 2005, 2006; Amberg et al., 2007). Interestingly, the opening of channels within the cluster, it is proposed, is coordinated so that each cluster functions as a unit (Navedo et al., 2005, 2007; Amberg et al., 2007). If correct, the opening and closing of individual ion channels within a cluster do not involve stochastic transitions between open and closed states, but the gating of one channel appears to determine the activity of its neighbors. Significantly, these clusters are constitutively active (Navedo et al., 2005) to create sites of nearly continual Ca^{2+} influx. The fluorescence manifestation of this continual influx of the ion, measured by Ca^{2+} indicators, has been called "persistent Ca^{2+} sparklets" (Navedo et al., 2005).

The coordinated opening and constitutive activity are unique behaviors of the voltage-dependent channel, which is induced by PKCα (Navedo et al., 2005). PKCα is localized to certain regions of the cell and presumably phosphorylates the Ca^{2+} channel to evoke constitutive channel opening at these sites (Navedo et al., 2005, 2006; Amberg et al., 2007). Constitutively active channel clusters have an open probability (0.18) ~10 million times higher than the average voltage-dependent Ca^{2+} channel (10^{-8}) at −70 mV (Navedo et al., 2005). Constitutive, rather than voltage-dependent, activity is proposed to largely determine the steady-state bulk average Ca^{2+} concentration ($[Ca^{2+}]_c$). At −70 mV, one to four clusters of constitutively active Ca^{2+} channels account for most of the steady-state Ca^{2+} entry in a typical cell (Navedo et al., 2005). At −40 mV, ~50% of the $[Ca^{2+}]_c$ may be derived from constitutive channel activity (Amberg et al., 2007). These interesting studies (Navedo et al., 2005, 2006, 2007; Amberg et al., 2007) suggest that constitutive channel opening is a fundamental property of the L-type Ca^{2+} channel (Navedo et al., 2006), a general mechanism for the control of Ca^{2+} in excitable cells (Navedo et al., 2006), and that its existence compels modification (Navedo et al., 2005) of our understanding of those stochastic processes that describe voltage-dependent Ca^{2+} channel behavior (Sakmann and Neher, 1995).

Here, we have addressed the contribution that constitutively active and voltage-dependent channels make to Ca^{2+} signaling in single smooth muscle cells by measuring near simultaneously (within 2 ms) bulk average and subplasma membrane $[Ca^{2+}]_c$. The occurrence of constitutive activity, as revealed by their fluorescence manifestation referred to as persistent Ca^{2+} sparklets, was examined using total internal reflection fluorescence microscopy (TIRF) and the contribution of constitutive and voltage-dependent channel activity to the maintenance of bulk average $[Ca^{2+}]_c$ determined using near simultaneously applied wide-field epifluorescence. A single

indicator was used to measure both subplasma membrane Ca^{2+} concentration ($[Ca^{2+}]_{PM}$) and bulk average $[Ca^{2+}]_c$. The use of a single indicator avoids those calibration problems that may arise when indicators of different rate constants are used to measure $[Ca^{2+}]$ in subplasma membrane space and bulk cytoplasm. For example, indicators with different association rate constants may report different $[Ca^{2+}]$ when the ion concentration changes rapidly where no differences exist.

The results here show that, in response to depolarization of the plasma membrane, the $[Ca^{2+}]$ rise that occurs in the different regions of the bulk cytoplasm is relatively uniform. In contrast, that of the subplasma membrane space is sporadic and uneven in time course and amplitude. The latter result suggests that active Ca^{2+} channels may be clustered in certain regions of the plasma membrane. Notwithstanding the apparent clustering of channels, constitutively active channels do not normally appear to contribute to Ca^{2+} signaling, and the repetitive localized $[Ca^{2+}]_{PM}$ rises that characterize persistent Ca^{2+} sparklets were seen rarely (2 of 306 cells). Inhibitors of voltage-dependent Ca^{2+} channels reduced neither the bulk average $[Ca^{2+}]_c$ at the resting potential (−70 mV) nor the $[Ca^{2+}]_c$ increase that follows an increase in electrochemical driving force on Ca^{2+} by hyperpolarization (−130 mV), an expectation if constitutively active channels determined $[Ca^{2+}]_c$. Nor did activation of PKC with phorbol ester–type tumor promoter indolactam-V induce constitutive activity in voltage-dependent Ca^{2+} channels at −70 or −130 mV. Thus, although voltage-dependent Ca^{2+} channels may be clustered in certain regions of plasma membrane, constitutively active channels appear to play little role in regulating $[Ca^{2+}]_c$; stochastic voltage-dependent behavior may be the predominant form of channel activity. The clustered voltage-dependent channels, by generating localized rises in subplasma membrane $[Ca^{2+}]$, may provide a mechanism to selectively activate various cellular processes in the subplasma membrane space.

MATERIALS AND METHODS

Cell isolation

Male guinea pigs (300–500 g) were humanely killed by cervical dislocation, followed by immediate exsanguination in accordance with the guidelines of the Animal (Scientific Procedures) Act UK 1986. A segment of intact distal colon (~5 cm) was transferred to oxygenated (95% O_2, 5% CO_2) physiological saline solution composed of (in mM): 118.4 NaCl, 25 $NaHCO_3$, 4.7 KCl, 1.13 NaH_2PO_4, 1.3 $MgCl_2$, 2.7 $CaCl_2$, and 11 glucose, pH 7.4. After removal of the mucosa from the tissue, single smooth muscle cells were enzymatically dissociated (McCarron and Muir, 1999).

The hepatic portal vein was excised, connective tissue and fat were removed, and the vessel was opened with a longitudinal incision and pinned on a Sylgard-coated (Corning) Petri dish. The tissue was bathed in the physiological saline solution. The endothelial layer was removed by rubbing with a cotton bud, the longitudinal layer was dissected away, and the circular smooth muscle layer was used to isolate single smooth muscle myocytes using a two-stage enzymatic dissociation. After dissection, the tissue was transferred to an isolation buffer containing (in mM): 80 Na glutamate, 55 NaCl, 6 KCl, 10 glucose, 10 HEPES, 1 $MgCl_2$, 1 $CaCl_2$, and 0.2 EDTA, pH 7.3 with NaOH. To isolate single smooth muscle cells, the tissue was incubated first for 12 min in isolation buffer that contained (in mg/ml): 1.64 bovine serum albumin, 1.7 papain, and 0.7 dithioerythritol. The tissue was then washed and transferred to isolation buffer that contained (in mg/ml): 1.64 bovine serum albumin, 2.2 collagenase type-F, and 0.7 hyaluronidase for 14 min. Finally, the tissue was again washed in isolation buffer and triturated gently to release single myocytes.

Cells were stored at 4°C and used within 24 h of cell isolation. All experiments were performed at room temperature (20 ± 2°C).

Electrophysiology

Membrane currents were measured using conventional tight-seal whole cell recording methods as described previously (McCarron et al., 2004, 2008; MacMillan et al., 2005; Chalmers and McCarron, 2008). The normal extracellular solution contained (in mM): 80 Na glutamate, 40 NaCl, 20 tetraethylammonium chloride, 1.1 $MgCl_2$, 3 $CaCl_2$, 10 HEPES, and 30 glucose, pH 7.4 with NaOH. A Ca^{2+}-free extracellular solution had the same composition, except there was no added Ca^{2+} and it contained additionally 10 mM EGTA. The pipette solution contained (in mM): 85 $(Cs)_2SO_4$, 20 CsCl, 1 $MgCl_2$, 30 HEPES, 3 MgATP, 2.5 pyruvic acid, 2.5 malic acid, 1 NaH_2PO_4, 5 creatine phosphate, and 0.5 guanosine phosphate. In some experiments (described in Results), the Ca^{2+} buffer EGTA (10 mM) was included in the patch pipette filling solution to limit the bulk average $[Ca^{2+}]_c$ rise. Whole cell currents were measured using an Axopatch 200B (MDS Analytical Technologies), low-pass filtered at 500 Hz, digitally sampled at 1.5 kHz using a Digidata interface and pClamp (version 10; MDS Analytical Technologies), and stored for analysis.

Imaging

Cells were loaded with 5 µM fluo-5F acetoxymethylester together with 10 µM wortmannin (to prevent contraction) for at least 20 min before the beginning of the experiment (McCarron et al., 2004, 2008; Chalmers and McCarron, 2008). In some experiments (described in Results), wortmannin was omitted from the loading solution; qualitatively identical results were obtained.

Bulk average $[Ca^{2+}]_c$ was measured using conventional wide-field epifluorescence and subplasma membrane $[Ca^{2+}]_{PM}$ using TIRF. TIRF uses evanescent wave illumination so that fluorescence may be visualized within ~100 nm of the plasma membrane (Axelrod, 2001; Beaumont, 2003). The improved axial resolution is provided by the control of the optical excitation penetration depth. In TIRF excitation, light is introduced with an angle of incidence sufficiently high to be reflected totally at the interface between the cover glass and bathing solution. The reflection generates an electromagnetic field in the aqueous medium that has a frequency identical to that of the incident light and an exponential intensity profile that is maximum at the glass–liquid interface. This "evanescent field" excites fluorophores in the immediate region near (~100 nm) the interface to offer a significant improvement in the ability to selectively image $[Ca^{2+}]$ changes derived from channel activity in the subplasma membrane space (Demuro and Parker, 2005, 2006).

The imaging system was constructed to enable through-the-objective TIRF and wide-field epifluorescence. To do this, a Nikon TE2000U inverted microscope with a dual-port epi-illuminator was custom fitted to enable rapid (2-ms) switching between laser (TIRF) and arc lamp (wide-field epifluorescence) illumination. This was accomplished by introducing a fiber-optically coupled laser beam via one port and an optical light guide–coupled 75W xenon arc lamp monchromator system (PTI Inc.) via the second

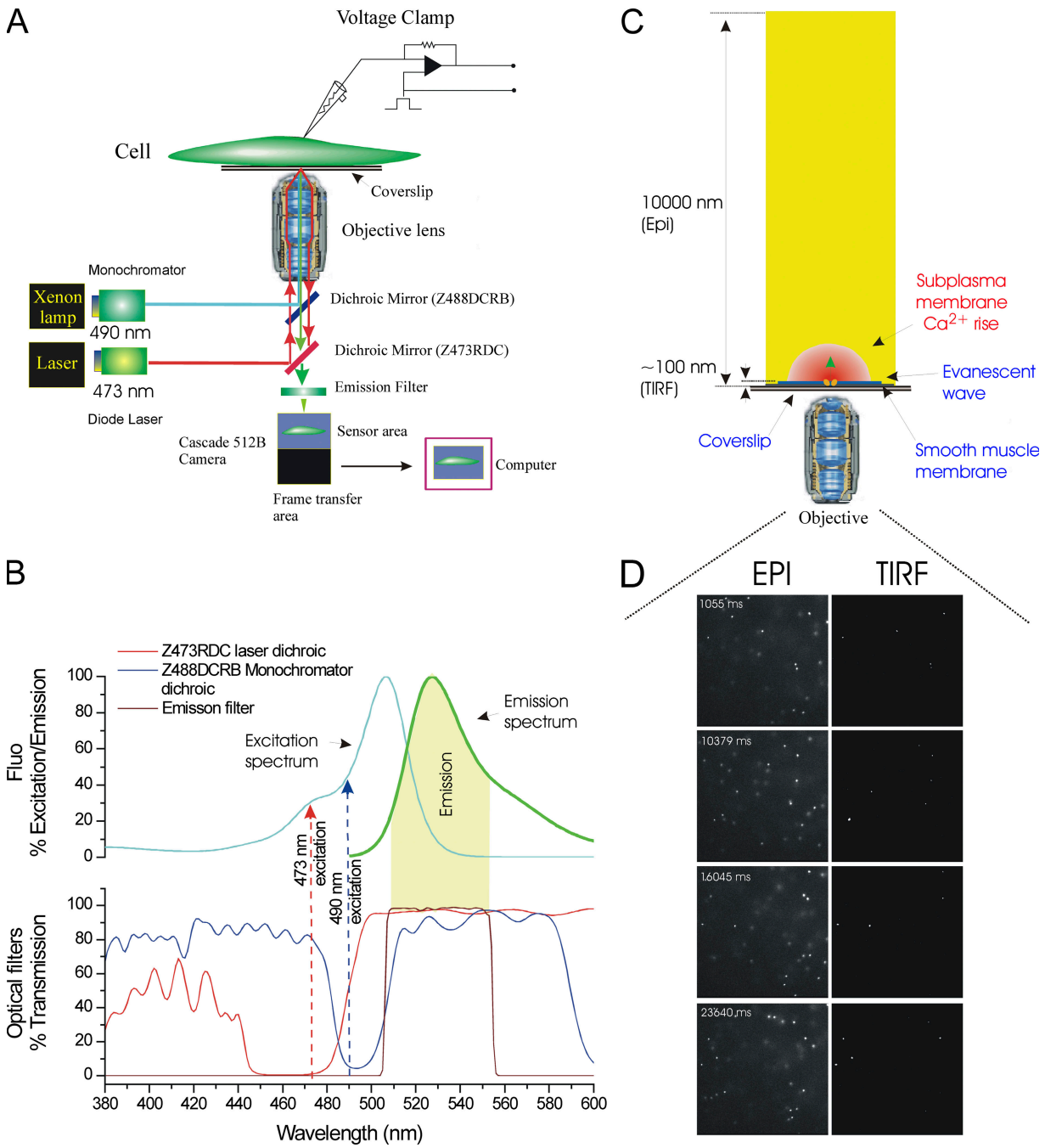

Figure 1. Schematic of the TIRF and wide-field epifluorescence system. (A) The experimental system was constructed around a Nikon TE2000U microscope; excitation and emission light paths are shown. Single cells were voltage clamped in whole cell configuration. Cells were loaded with fluo-5F and illuminated by two separate excitation sources (at 490 and 473 nm) via a dual epi-illuminator. The first wavelength (490 nm, bandpass 5 nm; blue) was provided by a monochromator and guided via a fiber-optic guide through a field stop diaphragm, a neutral density filter, and a HQ480/40 excitation filter (not depicted) before being reflected off a custom-made long-pass dichroic mirror (Z488DCRB). The latter was transmissive in the ranges of 380–480 and 506–589 nm and reflective from 485 to 499 nm (B). The second excitation wavelength (473 nm; red) for TIRF illumination was provided by a blue diode-pumped laser and guided via a fiber-optic coupling through an iris. The 473-nm light was then reflected off a dichroic mirror (Z473RDC) and transmitted through the upper dichroic (Z488DCRB; A and B) and focused to a spot on the back focal plane of the objective lens (Nikon 60×; oil immersion, NA 1.49). The laser-focusing lens was mounted on a micrometer-driven translation system so that the laser beam could be adjusted to enter the periphery of the objective aperture to achieve total internal reflection at the interface between the cover glass and the aqueous bathing medium. Fluorescence excited in the specimen by the evanescent wave or wide-field epi-illumination was collected through the objective lens, passed through the dichroic mirrors and a barrier filter, and imaged by a Phometrics Cascade 512B camera (Roper Scientific). The camera uses a back-illuminated frame transfer CCD with on-chip electron. (C) Enlarged view illustrating the imaging of near membrane Ca^{2+} from the microdomain (red) around a single open channel by evanescent wave (blue) formed by the TIRF objective lens

port. The laser (Oxxius; Laser 2000 UK), an air-cooled all-solid–state diode-pumped frequency and doubled Nd:YLF device, provided a wavelength of 473 nm (40 mW) for TIRF illumination and had a noise of <0.01% rms from 1 Hz to 10 MHz. The TEMoo output was coupled into a single-mode optical fiber with a numerical aperture of 0.1 and a core diameter of 3 µm. After collimation and reimaging through the Nikon TIRF attachment, the laser excitation was directed to the objective by a dichroic mirror (Z473RDC; Chroma Technology Corp.) (Fig. 1). A 60× 1.49-NA Nikon Plan Apo objective lens allowed the laser beam to be introduced at the outer edge of the objective aperture to achieve a high angle of incidence of the beam on the coverslip surface. The position of the beam was adjusted via a micrometer mounted on the TIRF unit (Nikon) that moved the fiber-optic coupler at its input into the illuminator. The angle of illumination was adjusted to exceed the critical angle to generate TIRF and an evanescent excitation field giving a penetration of ∼100 nm. To determine optimal imaging conditions, a test sample that consisted of sub-resolution fluorescent beads bathed in fluorescein was imaged. This sample allowed imaging parameters (illumination angle and intensity) that produced maximum image contrast to be determined and an illumination field that was generally even to be generated.

Wide-field epifluorescence excitation illumination was provided by the arc lamp, with the wavelength controlled via a monochromator (PTI Inc.) to give 490 nm (bandpass, 5 nm) coupled via a liquid light guide. The monochromator excitation wavelengths were directed to the objective by a custom-designed interference filter (Z488DCRB; Chroma Technology Corp.) (Fig. 1).

Fluorescence emission from the smooth muscle cell was collected by the objective lens, selected by a barrier filter (D535-40m; Fig. 1), and transmitted to a cooled, back-illuminated frame transfer CCD camera with on-chip electron multiplication (Cascade 512B; Photometrics Tuscan) controlled by EasyRatio pro software (1.2.1.87; PTI Inc.). Images were acquired sequentially with alternating laser and monochromator illumination at a frequency of 52 Hz unless otherwise indicated. In some experiments, TIRF alone was measured (at frequencies between 50 and 75 Hz), but no differences were observed in the subplasma membrane $[Ca^{2+}]$ measurements.

Electrophysiological measurements and imaging data were synchronized by recording, on pClamp, a transistor logic output from the CCD camera, which reported both its frame capture and readout status together with the electrophysiological information.

Immunoblotting

Freshly isolated colon and portal vein were homogenized in five volumes of ice-cold buffer (20 mM Tris-HCl, pH 7.4, 1 mM DTT, and 1× protease inhibitors; protease inhibitor cocktail set V, EDTA-free; EMD) using an Ultra-Turrax. Total protein content of tissue homogenates was measured by a Bradford assay using Coomassie Plus Reagent (Perbio). SDS-PAGE was performed as described previously (Currie et al., 2005) using 3–8% Tris-acetate gels for $Ca_V1.2$ separation and 10% Bis-Tris gels for PKCα separation (Invitrogen). After protein transfer onto nitrocellulose membranes, $Ca_V1.2$ was detected using a rabbit anti-$Ca_V1.2$ affinity-purified polyclonal antibody (Millipore) at a 1:500 dilution, followed by anti–rabbit IgG peroxidase conjugate (Sigma-Aldrich) at 1:5,000 dilution. $Ca_V1.2$ from rabbit cardiac homogenate was used as a positive control. PKCα was detected using a mouse anti-PKCα monoclonal IgG_1 (Millipore) at 1:1,000 dilution, followed by anti–mouse IgG peroxidase conjugate (GE Healthcare) at 1:5,000 dilution.

Data analysis

$[Ca^{2+}]$ images were analyzed using the program Metamorph 7.5 (MDS Analytical Technologies). To compensate for variations in fluorescence across the imaging field, e.g., from interference patterns from the glass coverslip and the coherent laser beam and irregularities in distance between the smooth muscle membrane and coverslip, fluorescence signals were background subtracted and expressed as ratios (F/F_0 or $\Delta F/F_0$) of fluorescence counts (F) relative to baseline (control) values (taken as 1) before stimulation (F_0). Original fluorescence recordings were not filtered, smoothed, or averaged.

Summarized results are expressed as means ± SEM of *n* cells. A paired or unpaired Student's *t* test was applied to the raw data as appropriate. $P < 0.05$ was considered significant.

Drugs and chemicals

Drugs were applied either by hydrostatic pressure ejection or addition to the extracellular solution as stated in Results. Concentrations in the text refer to the salts where appropriate. Ryanodine was purchased from Enzo Biochem, Inc. Fluo-5F acetoxymethylester was purchased from Invitrogen. All other reagents were purchased from Sigma-Aldrich.

RESULTS

An important aspect of this study was to ensure cells were in contact with the glass coverslip at the bottom of the dish. Cells were allowed to settle and then voltage clamped in whole cell configuration. Many cells that had been voltage clamped were rejected because they failed to show fluorescence in TIRF, even though fluorescence occurred in wide-field epifluorescence. The absence of fluorescence in TIRF suggests that those cells had not come into contact with the glass coverslip sufficiently well to bring the cytosol within the evanescent field. In cells where TIRF fluorescence was evident, fluorescence did not occur throughout but over restricted regions (20–80 µm) of the cell presumably because the cell had uneven contact with the coverslip. Measurements were restricted to the areas visible in TIRF.

Depolarization (−70 to +10 mV) activated a voltage-dependent Ca^{2+} current and increased $[Ca^{2+}]_c$ (Fig. 2). The increase in $[Ca^{2+}]_c$ measured in the bulk cytoplasm by wide-field epifluorescence occurred approximately uniformly and simultaneously throughout the cell (Fig. 2); i.e., the time course of the rise, the peak amplitude, and the rate of recovery of $[Ca^{2+}]_c$ to baseline values after the end of depolarization in different regions of the cell

and the simultaneously measured wide-field epifluorescence depth of field. The depth of the TIRF field was ∼100 nm, and that of the wide-field epi-fluorescent field was ∼10,000 nm. (D) Single-image frames of sub-resolution (100 nm) fluorescent latex beads floating in solution obtained in TIRF (right) and wide-field epifluorescence (left). Under wide-field epi-illumination (D, EPI, left), sub-resolution fluorescent latex beads floating in solution are illuminated through the field. Individual beads drift through Brownian motion. In TIRF illumination (D, TIRF, right), beads are illuminated only when they are within the evanescent field, i.e., within ∼100 nm of the coverslip. Beads diffusing in and out of the evanescent field appear and disappear suddenly.

did not differ significantly from each other (Table I). On the other hand, the increase in $[Ca^{2+}]_{PM}$ measured by TIRF was, in some regions, neither uniform nor simultaneous (Fig. 2 F). In these regions, the time course of the rise, the peak amplitude, and the rate of recovery of $[Ca^{2+}]_{PM}$ to baseline values after the end of depolarization differed significantly from the average $[Ca^{2+}]_{PM}$ values and those in identical regions of the bulk cytoplasm

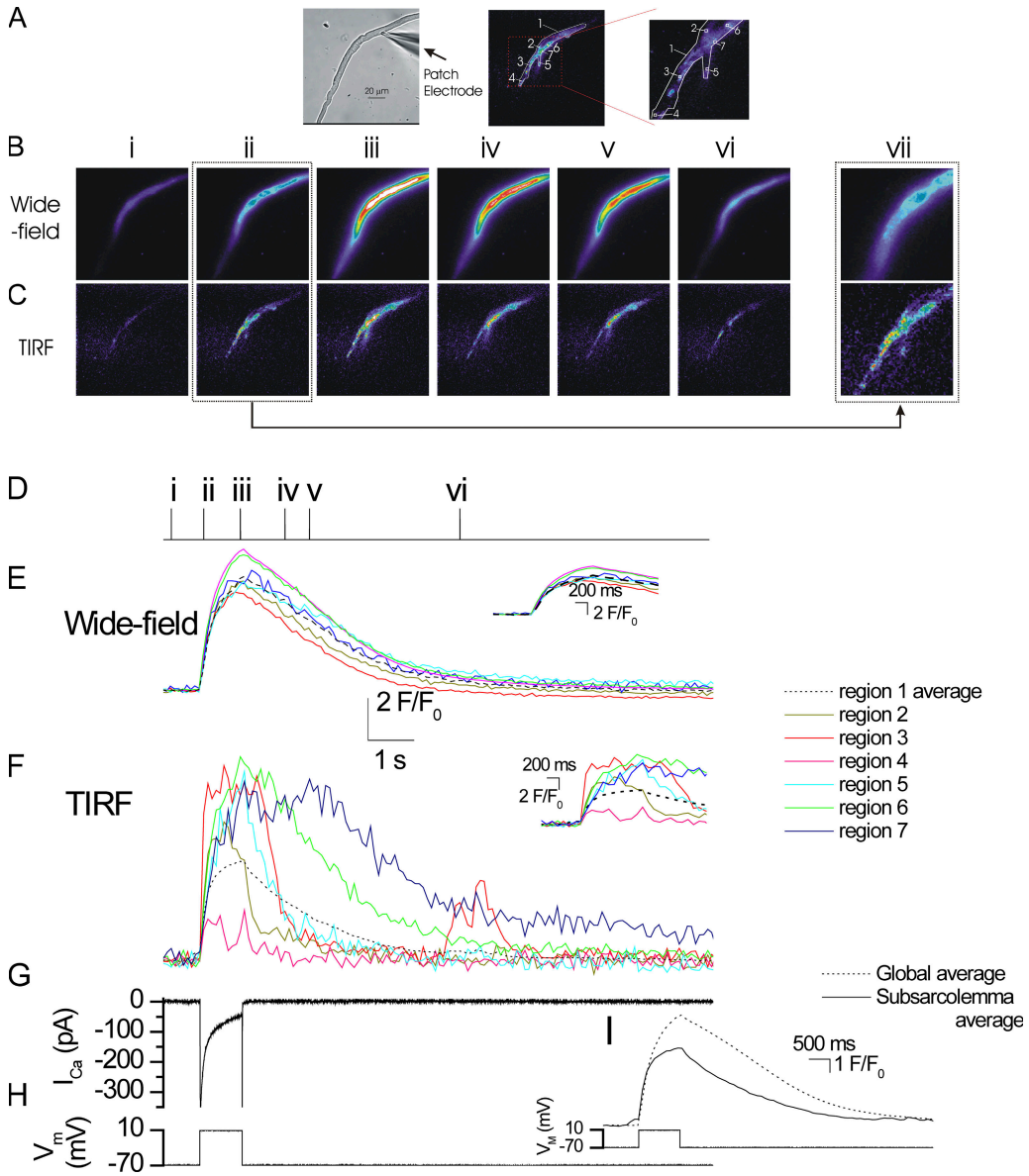

Figure 2. Simultaneous wide-field epifluorescence and TIRF $[Ca^{2+}]$ measurements in voltage-clamped single colonic myocytes. Depolarization (−70 to +10 mV; H) activated a voltage-dependent Ca^{2+} current (I_{Ca}; G) to evoke a rise in $[Ca^{2+}]$ (B, C, E, and F). The rise in $[Ca^{2+}]$, which occurred in the subplasma membrane space (measured by TIRF; C and F), was more rapid in onset than that seen in the bulk cytoplasm (measured by wide-field epifluorescence; B and E). The $[Ca^{2+}]$ images (B and C) are derived from the time points indicated by the corresponding numerals in D. $[Ca^{2+}]$ changes in B and C are represented by color: blue low and red/white high $[Ca^{2+}]$. The images (B and C) were taken before (i), during (ii and iii), and after (iv–vi)depolarization and show the resulting $[Ca^{2+}]$ changes. Changes in the fluorescence ratio with time (E and F) are derived from 2 × 2–pixel boxes (regions 1–6 in A, middle and right (expanded) panels, drawn at a 3 × 3–pixel size to facilitate visualization) and from a larger region encompassing the entire TIRF region (region 1). The latter was used to obtain an average subplasma membrane and bulk average $[Ca^{2+}]_c$ increase (I). Significantly, although the $[Ca^{2+}]_c$ increase that occurred in the bulk cytoplasm (B and E) was approximately uniform and simultaneous throughout the cell, those in the subplasma membrane space (C and F) had a wide range of amplitudes and various time courses. Note the spark-like events in region 3 toward the end of the recording. (A; left) A bright field image of the cell; see also whole cell electrode (right side). Insets in E and F show the rising phase of the transients on an expanded time base. For comparison, I shows the average subplasma membrane and bulk average $[Ca^{2+}]_c$ rise as measured in region 1 (A, right). B and C (VII) show an enlargement of ii to illustrate the localized nature of the rise in $[Ca^{2+}]$ in the subplasma membrane space.

TABLE I

Comparison of the [Ca^{2+}] changes that occurred in some regions of the subplasma membrane space and bulk cytoplasm

Subplasma membrane space	Peak $[Ca^{2+}]_{PM}$ ($\Delta F/F_0$)	Rise time (ms)	Rise slope ($\Delta F/F_0$/s)	Decay time (ms)	Decay slope ($\Delta F/F_0$/s)	*n*
Average	5.2 ± 0.7	320 ± 69	12.8 ± 2.2	3,730 ± 2,346	−1.5 ± 0.4	6
Regions	7.3 ± 1.4	118 ± 18	41 ± 10.9	851 ± 149	−5.9 ± 1.3	14
Bulk cytoplasm	Peak $[Ca^{2+}]_c$ ($\Delta F/F_0$)	Rise time (ms)	Rise slope ($\Delta F/F_0$/s)	Decay time (ms)	Decay slope ($\Delta F/F_0$/s)	*n*
Average	6.8 ± 1.2	343 ± 46	17.8 ± 5.2	3,496 ± 1,141	−2.0 ± 0.7	6
Regions	7.2 ± 0.6	345 ± 30	17.9 ± 3.2	2,992 ± 322	−1.7 ± 0.2	14

The rise time, rise slope, decay time, and decay slope were measured from the changes that occurred between 20 and 80% of the peak $\Delta F/F_0$ values. The "average" value has been derived from the entire region that was visible in TIRF. That area was used to generate an "area of interest," which was applied to obtain the average change that occurred in the bulk cytoplasm as measured in wide-field epifluorescence. "Regions" were 2 × 2–pixel areas. Rates of change in regions of the subplasma membrane space were substantially faster than those occurring in the same regions in the bulk cytoplasm. *n* values are from six different cells.

(Fig. 2 and Table I). Here, $[Ca^{2+}]_{PM}$ increases appeared as localized (3-µm) bright spots (Fig. 2 F) with faster than average rates of rise and decline (Table I). In other regions of the subplasma membrane space (e.g., region 7 in Fig. 2 F), the $[Ca^{2+}]_{PM}$ remained elevated after the depolarization had ended. Presumably, restricted diffusion slowed the rate at which Ca^{2+} could be cleared.

The localized $[Ca^{2+}]_{PM}$ increases were not visible in wide-field epifluorescence imaging (Fig. 2 E and Table I), even though measurements were derived from the same 2 × 2–pixel regions in which they appeared in TIRF. The fluorescence averaging that occurs over the much larger depth of field (10 µm) in wide-field epifluorescence presumably obscured the fast localized changes occurring in the subplasma membrane space.

In a substantial part of the subplasma membrane space, localized rises were not measured and a more uniform increase in $[Ca^{2+}]_{PM}$ occurred. Indeed, it is interesting that the average $[Ca^{2+}]_{PM}$ rise did not differ substantially from the bulk average $[Ca^{2+}]_c$ change (Fig. 2 I and Table I). Perhaps the bulk of the subplasma membrane space was receiving Ca^{2+} by diffusion so that the average rate of rise there was similar to that of the bulk cytoplasm that receives Ca^{2+} by diffusion alone.

Regional variation in the Ca^{2+} buffer capacity seems an unlikely explanation for the localized depolarization-evoked $[Ca^{2+}]_{PM}$ rises in the subplasma membrane space during rapid depolarization. Variations in the local $[Ca^{2+}]_{PM}$ were maintained when $[Ca^{2+}]$ was increased slowly (Fig. 3) by gradual changes in the membrane potential. During the slow changes in $[Ca^{2+}]_{PM}$, the buffers would have adequate time to reach equilibrium, yet transient local rapid $[Ca^{2+}]$ rises remain. Fig. 3 shows an example cell gradually depolarized (−20 mV) from the resting potential (−70 mV). Three illustrative cell areas show a region with localized changes (region 2), a region without localized changes (region 3), and the average $[Ca^{2+}]_{PM}$ change (region 1; note the ordinate scale change). The $[Ca^{2+}]_{PM}$ changes that occurred in region 3, which lacked localized increases, were similar to the average increase (region 1). On repolarization (−70 mV), the localized rises (region 2) ceased abruptly, whereas those of the average (region 1) and region 3 declined more slowly. The abrupt cessation suggests that plasma membrane channel activity, rather than "store-overload"–evoked Ca^{2+} release, accounts for the Ca^{2+} rise because the latter persists for tens of seconds after repolarization (MacMillan et al., 2005). A subsequent rapid depolarization (−70 to 0 mV) activated I_{Ca} and evoked an abrupt rise in $[Ca^{2+}]_{PM}$ that, in region 2, declined rapidly, whereas in regions 1 (average) and 3, a more gradual decline occurred. Interestingly, region 2, which exhibited rapid changes on depolarization, showed a relatively small $[Ca^{2+}]_{PM}$ increase to the RYR activator, caffeine (10 mM). Conversely the region (3) with the relatively small change on depolarization had a large response to caffeine (Fig. 3). This latter result again suggests that localized release from RYR is an unlikely explanation for the localized rises. Indeed, in other experiments, depletion of the SR of Ca^{2+} (using 50 µM ryanodine and repetitive application of 10 mM caffeine) neither reduced the depolarization-evoked $[Ca^{2+}]_{PM}$ or $[Ca^{2+}]_c$ increase (Fig. 4 and Table II). Thus, in control, depolarization (−70 to +10 mV) evoked a $[Ca^{2+}]$ rise in the bulk cytoplasm (5.1 ± 0.9 $\Delta F/F_0$) and subplasma membrane space (4.7 ± 1.2 $\Delta F/F_0$). 10 mM caffeine (3 s by pressure ejection) also evoked a $[Ca^{2+}]$ rise in the bulk cytoplasm (8.8 ± 3.3 $\Delta F/F_0$) and in the subplasma membrane space (7.0 ± 2.6 $\Delta F/F_0$; $n = 4$). After 50 µM ryanodine, the caffeine-evoked $[Ca^{2+}]$ rise declined to 0.31 ± 0.5 ($\Delta F/F_0$) in the bulk cytoplasm and 0.2 ± 0.7 ($\Delta F/F_0$; $n = 4$) in the subplasma membrane space after three caffeine applications (each 10 mM for 3 s, with 90 s between applications). After inhibition of the caffeine-evoked $[Ca^{2+}]$ increase, the depolarization-evoked $[Ca^{2+}]$ rise in the bulk cytoplasm (6.6 ± 1.6 $\Delta F/F_0$) and subplasma membrane space (5.1 ± 0.8 $\Delta F/F_0$) were not reduced and, indeed, may have increased in the bulk cytoplasm as reported previously (Bradley et al., 2004). This result suggests that Ca^{2+} release from the SR does

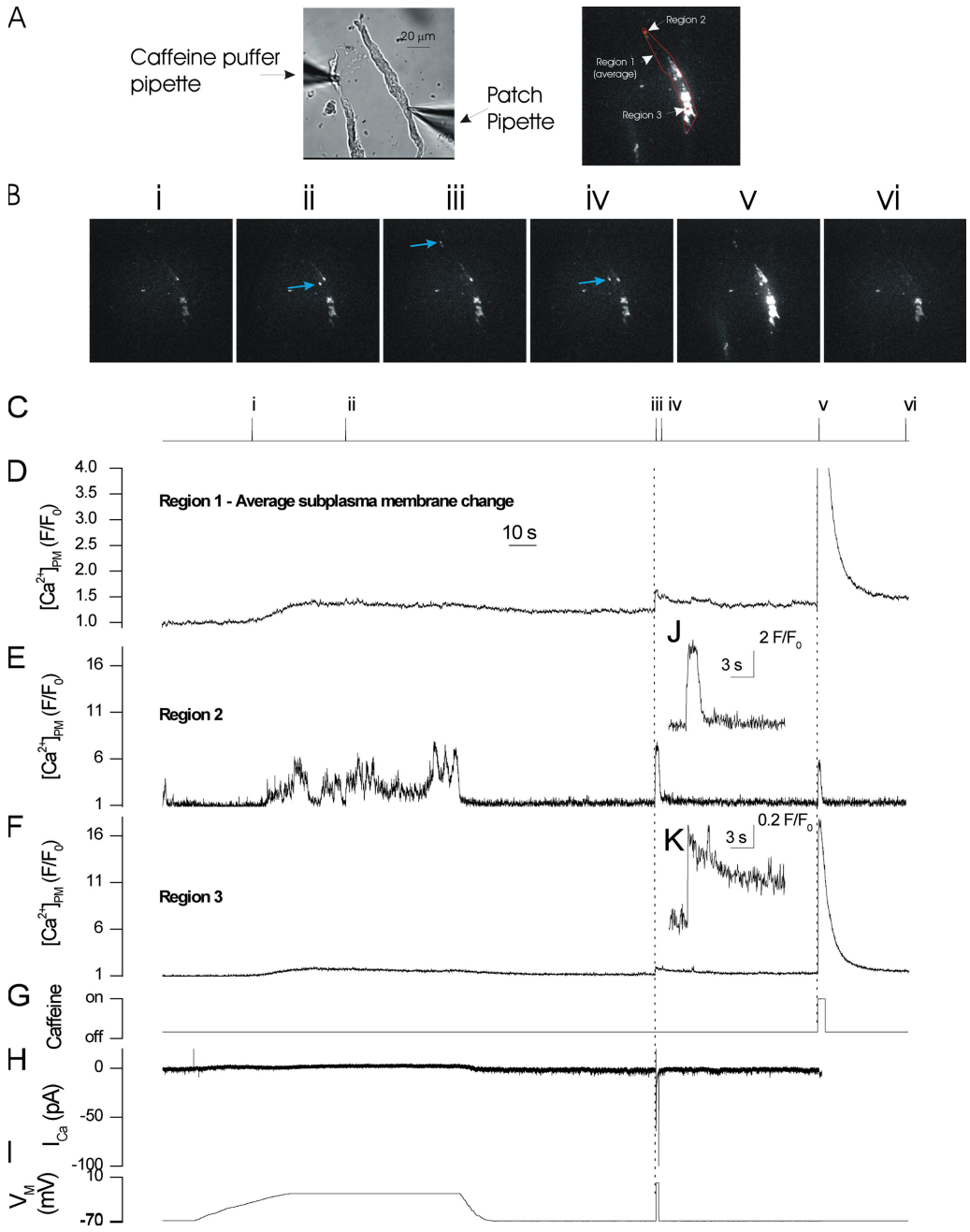

Figure 3. Local subplasma membrane Ca^{2+} transients in response to plasma membrane depolarization and caffeine in a voltage-clamped single colonic myocyte. Gradual depolarization from −70 to −20 mV (I) elevated $[Ca^{2+}]$ in the subplasma membrane space as measured in TIRF (D–F). The $[Ca^{2+}]$ increase was more localized and substantially larger in some regions than others (compare E and F). Two example regions (regions 2 and 3) are shown (E and F); localized rises occurred in region 2, but not region 3. Blue arrows in the frames in B (ii–iv) show examples of the localized rises in $[Ca^{2+}]$. The $[Ca^{2+}]$ increase that occurred in region 3 (F) was slow and of smaller magnitude than that of region 2 (E). When the membrane potential was restored to −70 mV (I), $[Ca^{2+}]$ was returned toward resting levels. A subsequent transient depolarization to 0 mV (I) activated voltage-dependent Ca^{2+} current (I_{Ca}; H) and increased $[Ca^{2+}]$ (D–F). The increase was larger and declined more rapidly in region 2 (E and inset J) than region 3 (F and inset K). Those regions (E, region 2) that showed large responses to depolarization had small responses to RYR activation by caffeine (G). Conversely, a large response (F, region 3) to caffeine (G) occurred in regions with small responses to depolarization. Region 1 (D) is a subplasma membrane average change. Numerals in images (B) correspond to those in C. Changes in the fluorescence ratio with time (D–F) are derived from 1-pixel boxes (regions 2 and 3, shown at 3 × 3 pixels to facilitate visualization) and from a larger region the entire TIRF image (region 1) to obtain an average subplasma membrane $[Ca^{2+}]$ change (D). The position of the regions from which the transients (D–F) were obtained are shown in A (right panel). A bright field image of the cell is shown in A (left panel); see also whole cell electrode (right side) and puffer pipette, which contained caffeine (10 mM; left side). The data in this figure is representative of three similar experiments.

TABLE II

Depletion of the SR does not reduce the [Ca^{2+}] increases in subplasma membrane space or bulk cytoplasm

Control		Peak [Ca^{2+}] ($\Delta F/F_0$)	Rise time (ms)	Rise slope ($\Delta F/F_0$/s)	Decay time (ms)	Decay slope ($\Delta F/F_0$/s)	*n*
Subplasma membrane space	Average	4.7 ± 1.2	312 ± 55	10.0 ± 5.1	3,236 ± 1,705	−2.0 ± 0.7	4
	Regions	6.2 ± 1.0	145 ± 30	31 ± 9.2	1,136 ± 221	−3.8 ± 0.7	8
Bulk cytoplasm	Average	5.1 ± 0.9	328 ± 55	10.7 ± 3.0	3,295 ± 1,759	-2.1 ± 0.7	4
	Regions	5.3 ± 0.7	320 ± 59	13 ± 3.4	3,187 ± 1,116	−2.3 ± 0.7	8
After SR depletion							
Subplasma membrane space	Average	5.1 ± 0.8	365 ± 84	11.6 ± 2.5	3,708 ± 2,290	−1.7 ± 0.6	4
	Regions	6.6 ± 0.7	133 ± 41	30 ± 7.7	1,040 ± 151	−3.1 ± 0.5	8
Bulk cytoplasm	Average	6.6 ± 1.6	372 ± 50	12.3 ± 1.2	3,868 ± 1,934	−1.9 ± 0.4	4
	Regions	6.8 ± 1.4	472 ± 152	19 ± 7.0	2,129 ± 496	−2.7 ± 0.9	8

SR depletion (using 50 µM ryanodine and repetitive application of 10 mM caffeine) neither reduced the depolarization-evoked $[Ca^{2+}]_{PM}$ or $[Ca^{2+}]_c$ increase. This result suggests that SR Ca^{2+} release does not contribute substantially to the depolarization-evoked $[Ca^{2+}]_{PM}$ or $[Ca^{2+}]_c$ increases. The rise time, rise slope, decay time, and decay slope were measured from the changes that occurred between 20 and 80% of the peak $\Delta F/F_0$ values. The "average" value has been derived from the entire region that was visible in TIRF. That area was used to generate an "area of interest," which was applied to obtain the average change that occurred in the bulk cytoplasm as measured in wide-field epifluorescence. "Regions" were 1-pixel areas.

not contribute substantially to the depolarization-evoked $[Ca^{2+}]_{PM}$ or $[Ca^{2+}]_c$ increases.

Collectively, the localized rise in $[Ca^{2+}]$ that occurs in the subplasma membrane space suggests that voltage-dependent Ca^{2+} channels are clustered in some regions of the plasma membrane. The activity of the clustered channels is controlled by membrane potential.

Constitutively active dihydropyridine-sensitive Ca^{2+} channels

Ca^{2+} entry through clusters of dihydropyridine-sensitive, constitutively active Ca^{2+} channels may, it is proposed, create sites of continual Ca^{2+} influx to determine the bulk average $[Ca^{2+}]_c$, even at the resting potential of −70 mV (Navedo et al., 2005). In the present study, although channels that appear to be clustered were observed (Figs. 2 and 3), constitutive channel activity was seen infrequently (2 of 306 cells). Fig. 5 shows an example of activity that is consistent with constitutive channel opening. The activity manifests as repetitive localized rises in $[Ca^{2+}]_c$ revealed by the occurrence of persistent Ca^{2+} sparklets (Navedo et al., 2005) (Fig. 5). The persistent Ca^{2+} sparklets were blocked rapidly by the dihydropyridine antagonist nimodipine (1 µM), applied by pressure ejection from a nearby "puffer" pipette. Interestingly, even though the $[Ca^{2+}]_{PM}$ rise from the persistent Ca^{2+} sparklet was blocked by nimodipine, the average subplasma membrane $[Ca^{2+}]_{PM}$ was unaltered. This latter result suggests that the localized rise from the Ca^{2+} sparklet does not significantly alter the average subplasma membrane $[Ca^{2+}]$.

The experimental conditions in the present study differ from those that were used to routinely record persistent Ca^{2+} sparklets (Navedo et al., 2005, 2006). In the latter experiments, there was a high concentration of Ca^{2+} indicator (200 µM; 5 µM was used in the present study). The present lower indicator concentration will minimize the attenuation of the $[Ca^{2+}]$ change caused by buffering and will not alter appreciably the equilibrium of Ca^{2+} with the endogenous buffers. Other differences were that a high $[Ca^{2+}]$ (20 mM) and SR Ca^{2+} pump inhibitor thapsigarin (1 µM) were present in the extracellular solution (Navedo et al., 2005, 2006). The pipette solution also contained a high concentration (10 mM) of the buffer EGTA (Navedo et al., 2005, 2006). Perhaps these conditions are required to measure persistent Ca^{2+} sparklets routinely. However, in another series of experiments (not depicted) in which 10 mM EGTA was included in the pipette filling solution (external $[Ca^{2+}]$ increased to 20 mM and 1 µM thapsigargin present in bath throughout), constitutive channel activity was not seen ($n = 6$). In a further series of experiments, coverslips on which the cells were settled were coated with poly-lysine (Navedo et al., 2005), but again sparklets were not observed ($n = 25$).

The rare observation of persistent Ca^{2+} sparklets may have occurred because only a small fraction of the cell was visible in TIRF. That is, persistent Ca^{2+} sparklets may normally be present in all cells but were not measured because they lay outside the region of the cell observed in TIRF. Alternatively, persistent Ca^{2+} sparklets may be an unusual form of Ca^{2+} channel activity. To distinguish between these possibilities, $[Ca^{2+}]$ was measured near simultaneously in the subplasma membrane space and bulk cytoplasm to determine the contribution persistent Ca^{2+} sparklets make to $[Ca^{2+}]_c$ values. The latter measurement is relevant particularly because the bulk average $[Ca^{2+}]_c$ at the resting membrane potential (−70 mV), at which voltage-dependent Ca^{2+} channels are largely closed, is suggested to be explained by Ca^{2+} entry via constitutively

active L-type Ca^{2+} channels (Navedo et al., 2005; Amberg et al., 2007). Constitutively active channels are, it is proposed, able to maintain Ca^{2+} influx at the negative membrane potential (−70 mV) because PKCα phosphorylation activates the channel regardless of membrane potential (Navedo et al., 2005, 2006; Amberg et al., 2007).

The contribution of constitutively active L-type Ca^{2+} channels to the bulk average $[Ca^{2+}]_c$

Two protocols have been used to examine the contribution of dihydropyridine-sensitive constitutively active channels to the maintenance of steady-state bulk average $[Ca^{2+}]_c$. First, the effects of a dihydropyridine blocker

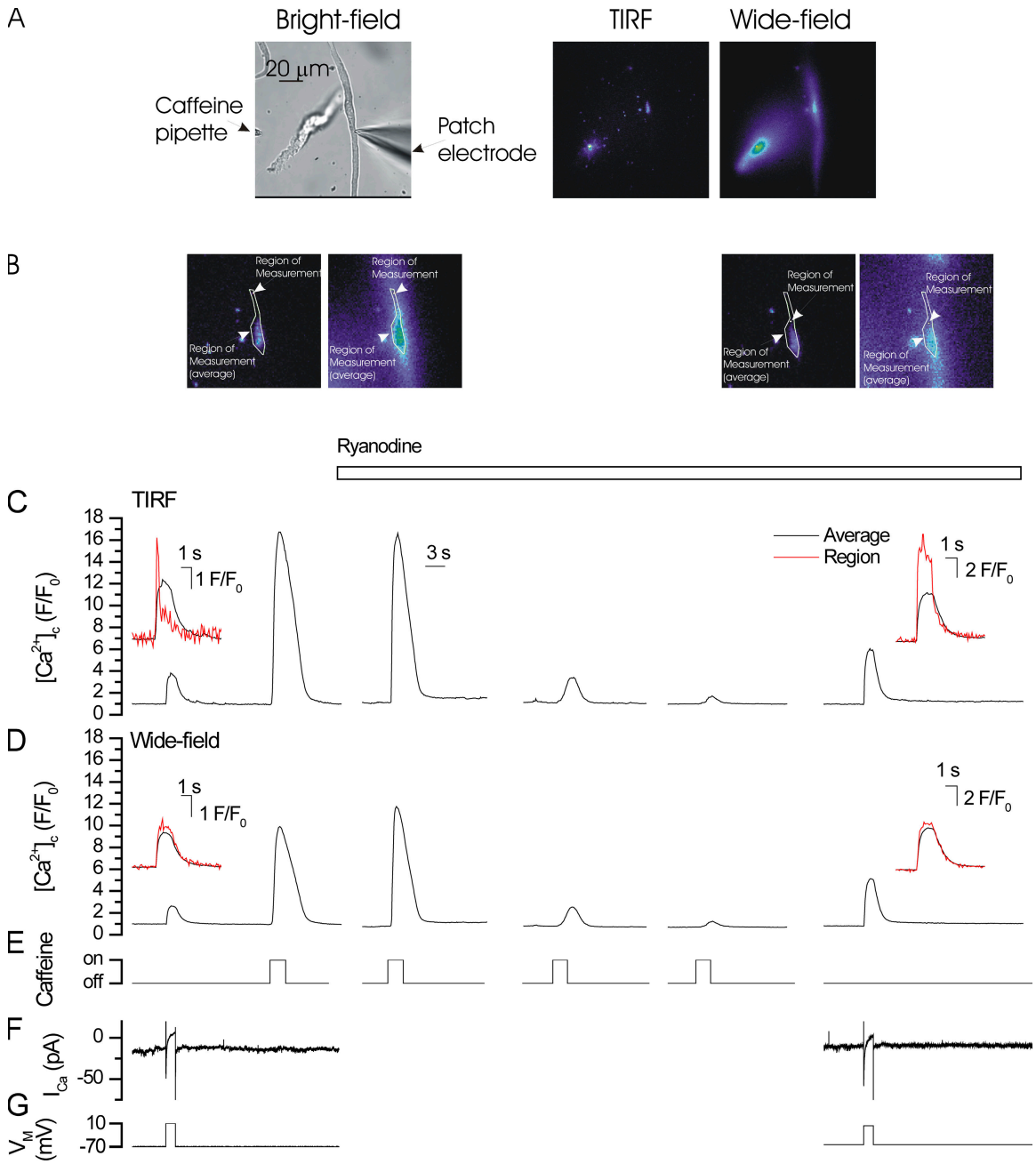

Figure 4. Depletion of the SR of Ca^{2+} changes does not reduce the $[Ca^{2+}]$ increases in subplasma membrane space or bulk cytoplasm in voltage-clamped single colonic myocytes. Depolarization (−70 to +10 mV; G) activated a voltage-dependent Ca^{2+} current (I_{Ca}; F) to evoke a rise in $[Ca^{2+}]$ (C and D). The rise in $[Ca^{2+}]$, which occurred in some regions (B, left panels) of the subplasma membrane space (measured by TIRF; red line in inset in C), were more rapid in both onset and decline than that seen in average measured in the subplasma membrane space (black red line in inset in C; B and E). The same regions in the bulk cytoplasm (measured by wide-field epi-florescence; B, left panels) had approximately comparable rates of rise and decline (D, inset). 10 mM caffeine (E) applied by pressure ejection from a puffer pipette (A, left side; see also whole cell patch electrode [right side]) evoked increases in $[Ca^{2+}]$ (C and D). 50 µM ryanodine (C, open bar above the trace) after repeated application of caffeine to open RYR abolished the $[Ca^{2+}]$ increase to caffeine presumably

of voltage-dependent Ca^{2+} channels, 1 μM nimodipine, on resting $[Ca^{2+}]_c$ was examined. Nimodipine blocks the open state of the dihydropyridine-sensitive voltage-dependent Ca^{2+} channel (Kd 0.02–0.5 nM) (Cohen and McCarthy, 1987; McCarthy and Cohen, 1989). If the dihydropyridine-sensitive channel determines resting values, the blocker will reduce $[Ca^{2+}]_c$. As a part of the protocol, the inhibitory efficacy of nimodipine on voltage-dependent Ca^{2+} channels was confirmed. In a second separate protocol, the effects of nimodipine on the Ca^{2+} influx that follows a prolonged (2.5-s) hyperpolarization to −130 mV was examined. Hyperpolarization increases the electrochemical driving force on Ca^{2+} to increase entry of the ion. If voltage-dependent Ca^{2+} channels are constitutively active they will remain so regardless of the membrane potential (because of PKCα phosphorylation), and nimodipine should reduce Ca^{2+} entry and $[Ca^{2+}]$ rise.

1 μM nimodipine, applied by pressure ejection from a nearby puffer pipette, rapidly blocked the Ca^{2+} current and rise in $[Ca^{2+}]_c$, but did not reduce $[Ca^{2+}]_c$ at the resting membrane potential (−70 mV) (Fig. 6). Thus, depolarization (−70 to +10 mV) activated a voltage-dependent Ca^{2+} current (I_{Ca}) and increased $[Ca^{2+}]_c$; the latter returned toward basal levels when the depolarization had ended (Fig. 6). Next, the blocker nimodipine (1 μM) was applied from the puffer pipette. Little change in $[Ca^{2+}]_c$ occurred. Resting bulk average $[Ca^{2+}]_c$ was 1.03 ± 0.026 before (F/F_0) 1 μM nimodipine and 0.99 ± 0.035 after (F/F_0; $n = 8$; $P > 0.05$) (Fig. 6). Neither did resting $[Ca^{2+}]_{PM}$ change before (1.1 ± 0.044 F/F_0) and after (1.04 ± 0.051 F/F_0; $n = 8$; $P > 0.05$) 1 μM nimodipine. Although nimodipine was ineffective in altering resting $[Ca^{2+}]_c$, I_{Ca} and its accompanying $[Ca^{2+}]_c$ increase were blocked (Fig. 6). Thus, in control, depolarization-evoked (−70 to +10 mV) I_{Ca} averaged −89 ± 21 pA and $[Ca^{2+}]$ rise in the bulk cytoplasm 4.1 ± 1.2 ($\Delta F/F_0$) and subplasma membrane space 4.7 ± 1.4 ($\Delta F/F_0$; $n = 8$). After 1 μM nimodipine, I_{Ca} (−13 ± 3 pA; $P < 0.01$) and the accompanying $[Ca^{2+}]$ rise in the bulk cytoplasm (0.37 ± 0.13 $\Delta F/F_0$; $P < 0.05$) and subplasma membrane space (0.49 ± 0.17 $\Delta F/F_0$; $n = 8$; $P < 0.05$) were each significantly reduced. After a further ∼3 min, I_{Ca} (−59 ± 23 pA) and the $[Ca^{2+}]_c$ rise in the bulk cytoplasm 2.3 ± 0.75 ($\Delta F/F_0$) and subplasma membrane space 3.1 ± 0.69 ($\Delta F/F_0$) each were restored toward control levels.

The Ca^{2+} indicator used in the present study (fluo-5F) was adequately sensitive to measure decreases in $[Ca^{2+}]$ from the resting value. A Ca^{2+}-free bath solution (containing 10 mM EGTA) applied (for ∼15 s) to the cell by pressure ejection from a puffer pipette resulted in a substantial fall in the resting $[Ca^{2+}]$. Thus, resting global $[Ca^{2+}]_c$ declined significantly ($P < 0.01$) from 0.99 ± 0.003 (F/F_0) to 0.75 ± 0.046 (F/F_0) in Ca^{2+}-free bath, and then recovered when the pressure ejection stopped to 0.95 ± 0.023 (F/F_0). In the subplasma membrane space, $[Ca^{2+}]_{PM}$ declined from a resting value of 0.99 ± 0.025 (F/F_0) to 0.72 ±0.055 (F/F_0) in Ca^{2+}-free bath, and then recovered to 1.08 ± 0.03 (F/F_0) when pressure ejection stopped ($n = 7$).

In the next protocol (Fig. 7), to determine whether or not constitutively active channels regulate bulk average $[Ca^{2+}]_c$, the electrochemical driving force for Ca^{2+} entry via voltage-dependent Ca^{2+} channels was increased by hyperpolarization to −130 mV (from −70 mV). A 60-mV hyperpolarization increases the electrochemical driving force acting on Ca^{2+} by an amount equivalent to a 100-fold increase in extracellular $[Ca^{2+}]$ (i.e., to 300 mM). Hyperpolarization (−130 mV) increased bulk average (0.66 ± 0.26 $\Delta F/F_0$) and subplasma membrane $[Ca^{2+}]$ (1.1 ± 0.44 $\Delta F/F_0$) (Fig. 7). The same hyperpolarization applied again some 60 s later evoked a comparable rise in $[Ca^{2+}]$ in the bulk cytoplasm (0.75 ± 0.31 $\Delta F/F_0$) and subplasma membrane space (1.03 ± 0.35 $\Delta F/F_0$) (Fig. 7). Next, in the same cell, the hyperpolarization protocol was repeated but, in this case, 1 μM nimodipine was applied to block voltage-dependent Ca^{2+} channels before the second hyperpolarization occurred (Fig. 7). In these experiments, hyperpolarization (to −130 mV from −70 mV) evoked an increase in $[Ca^{2+}]_c$ (0.77 ± 0.24 $\Delta F/F_0$) and $[Ca^{2+}]_{PM}$ (0.82 ± 0.24 $\Delta F/F_0$; $n = 5$). 1 μM nimodipine blocked neither the hyperpolarization-evoked increase in the bulk cytoplasm (0.99 ± 0.35 $\Delta F/F_0$; $n = 5$; $P > 0.05$) nor subplasma membrane space (1.1 ± 0.34 $\Delta F/F_0$; $n = 5$; $P > 0.05$) (Fig. 7). This experiment suggests that constitutively active dihydropyridine-sensitive Ca^{2+} channels do not play a major role in regulating bulk average $[Ca^{2+}]_c$.

Wortmannin, present in the loading solution (see Materials and methods), is a kinase inhibitor (e.g., myosin

because of SR store depletion. In contrast, the depolarization-evoked $[Ca^{2+}]$ increase was not reduced in either subplasma membrane space or bulk cytoplasm. After inhibition of the caffeine-evoked $[Ca^{2+}]$ increase, the depolarization-evoked $[Ca^{2+}]_{PM}$ or $[Ca^{2+}]_c$ increase were not reduced. Furthermore, localized increases in regions of the subplasma membrane space measured by TIRF (red line in inset in C) were more rapid in onset and decline than those seen in average measured in the subplasma membrane space (black red line in inset in C; B and E). This result suggests that SR Ca^{2+} release does not contribute substantially to the depolarization-evoked $[Ca^{2+}]_{PM}$ or $[Ca^{2+}]_c$ increases. Changes in the fluorescence ratio with time (C and D) are derived from 1-pixel boxes (B) and from a larger region encompassing the entire TIRF region (B). The latter was used to obtain an average subplasma membrane and bulk average $[Ca^{2+}]$ increases (C and D). (A; left) A bright field image of the cell; see also whole cell electrode (right side). B shows an expanded view of A (middle and right panels) to illustrate the regions of measurement. Note the pixel position is in a different position after SR depletion. The cell moved slightly during solution exchanges, and a new voltage-dependent Ca^{2+} channel cluster may have emerged.

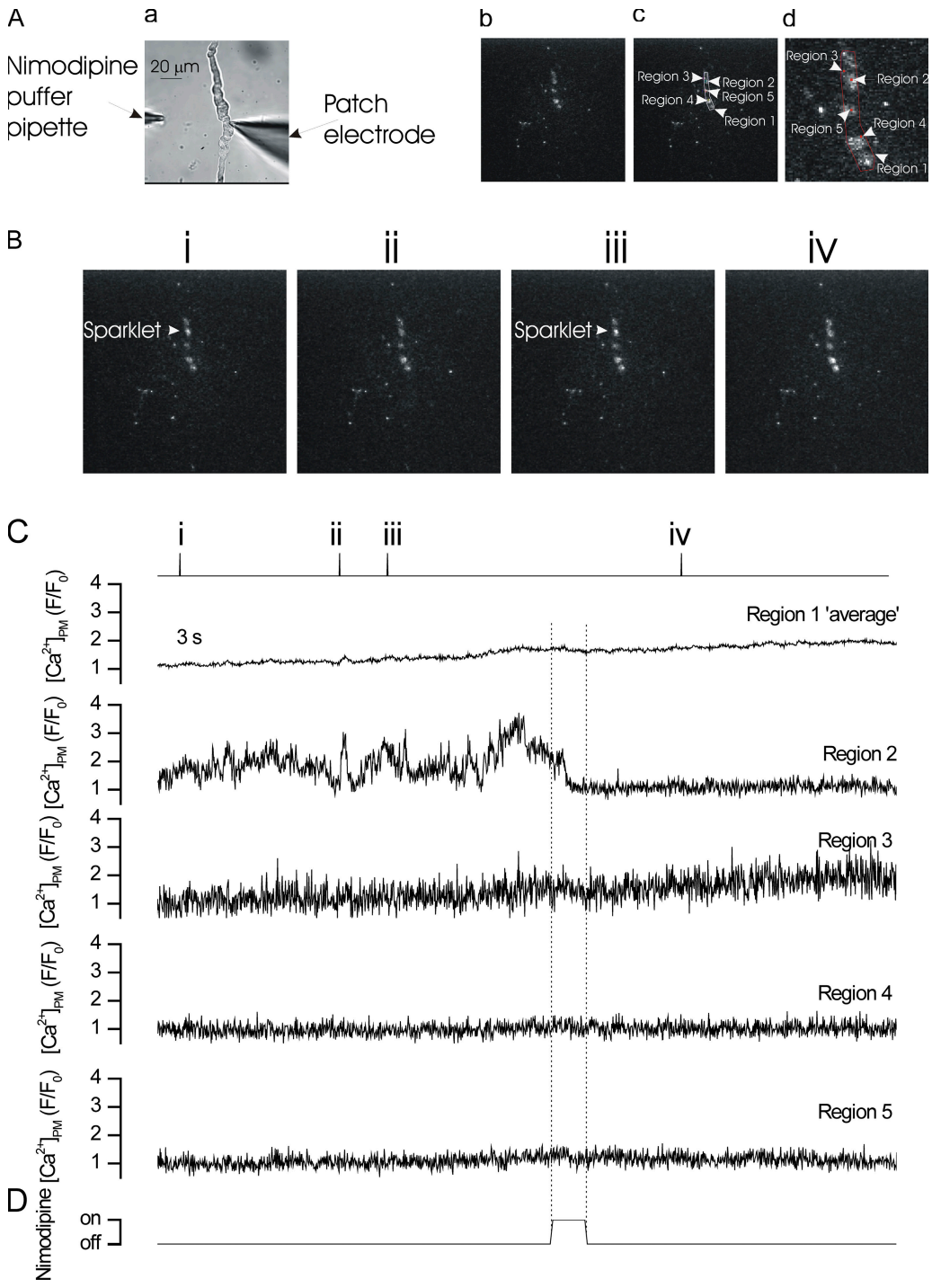

Figure 5. Persistent Ca^{2+} sparklets in a voltage-clamped single colonic myocyte. At −70 mV, persistent Ca^{2+} influx occurred in one site (C, region 2) of the cell as measured in TIRF and revealed by the occurrence of persistent Ca^{2+} sparklets. The dihydropryidine blocker of L-type voltage-dependent Ca^{2+} channels, nimodipine (1 μM), applied from a puffer pipette (D) abruptly halted sparklet activity. The latter result suggests that sparklets were derived from the activity of L-type Ca^{2+} channels. Nimodipine produced little change in $[Ca^{2+}]$ in other regions (1 and 3–5) of the cell. The $[Ca^{2+}]_{PM}$ images (B) were derived from the time points indicated by the corresponding numerals in C. Changes in the fluorescence ratio with time (C) were derived from 1-pixel boxes (Regions 2–5 in A c and expanded view in A d) and from a larger region encompassing the part of the cell in TIRF (Region 1; A, c and d). The latter was used to obtain an average subplasma membrane $[Ca^{2+}]_{PM}$ change (C). (A, a) A bright field image of the cell; see also whole cell electrode (right side) and 1 μM nimodipine–containing puffer pipette. Persistent Ca^{2+} sparklets were seen in 2 of 306 cells.

light chain kinase and phosphatidylinositol 3-kinase) and could have prevented persistent Ca^{2+} sparklets from developing. In a separate series of experiments (not depicted), as a control, wortmannin was omitted from the cells during Ca^{2+} indicator loading and the hyperpolarization protocol was repeated. In these experiments, the hyperpolarization (to −130 mV from −70 mV) evoked a $[Ca^{2+}]$ rise in the subplasma plasma membrane space (0.32 ± 0.19 $\Delta F/F_0$; n = 4) and bulk cytoplasm (0.31 ± 0.19 $\Delta F/F_0$; n = 4). 1 µM nimodipine blocked neither the hyperpolarization-evoked $[Ca^{2+}]_c$ increase in the subplasma membrane space (0.84 ± 0.52 $\Delta F/F_0$; n = 4) nor bulk cytoplasm (0.85 ± 0.5 $\Delta F/F_0$; n = 4; P > 0.05) (not depicted). Again, this experiment suggests that those channels that control bulk average $[Ca^{2+}]_c$ were not constitutively active dihydropyridine-sensitive channels.

Role of PKCα in inducing constitutive activity in voltage-dependent Ca^{2+} channels

PKCα is required to evoke constitutive activity in $Ca_V1.2$ voltage-dependent Ca^{2+} channels (Navedo et al., 2005, 2006; Amberg et al., 2007). PKCα and $Ca_V1.2$ voltage-dependent Ca^{2+} channels are each expressed in the smooth muscle cells being studied (Fig. 8, A and B). To test the proposal that PKCα may induce constitutive activity, the PKC activator indolactam-V (10 µM) was applied to the cells and the voltage protocols (Figs. 6 and 7) were repeated. In these experiments, depolarization (−70 to +10 mV) activated a voltage-dependent Ca^{2+} current (I_{Ca}) and increased $[Ca^{2+}]_c$; the latter returned toward basal levels when the depolarization ended (Fig. 8 C) (I_{Ca} in indolactam was significantly [P < 0.05] greater than in its absence, as expected from the effects of PKC on voltage-dependent Ca^{2+} channels [e.g., Vivaudou et al., 1988]). Next, the blocker nimodipine (1 µM) was applied from the puffer pipette but again produced no significant change in $[Ca^{2+}]_c$. Thus, in control, resting bulk average $[Ca^{2+}]$ was 1.1 ± 0.09 (F/F_0), whereas after 1 µM nimodipine it was 1.1 ± 0.09 (F/F_0; n = 8; P > 0.05). Resting subplasma membrane $[Ca^{2+}]$ in control was 1.16 ± 0.08 (F/F_0), and after 1 µM nimodipine it was 1.18 ± 0.08 (F/F_0; n = 8; P > 0.05) (Fig. 8 C). In contrast, I_{Ca}

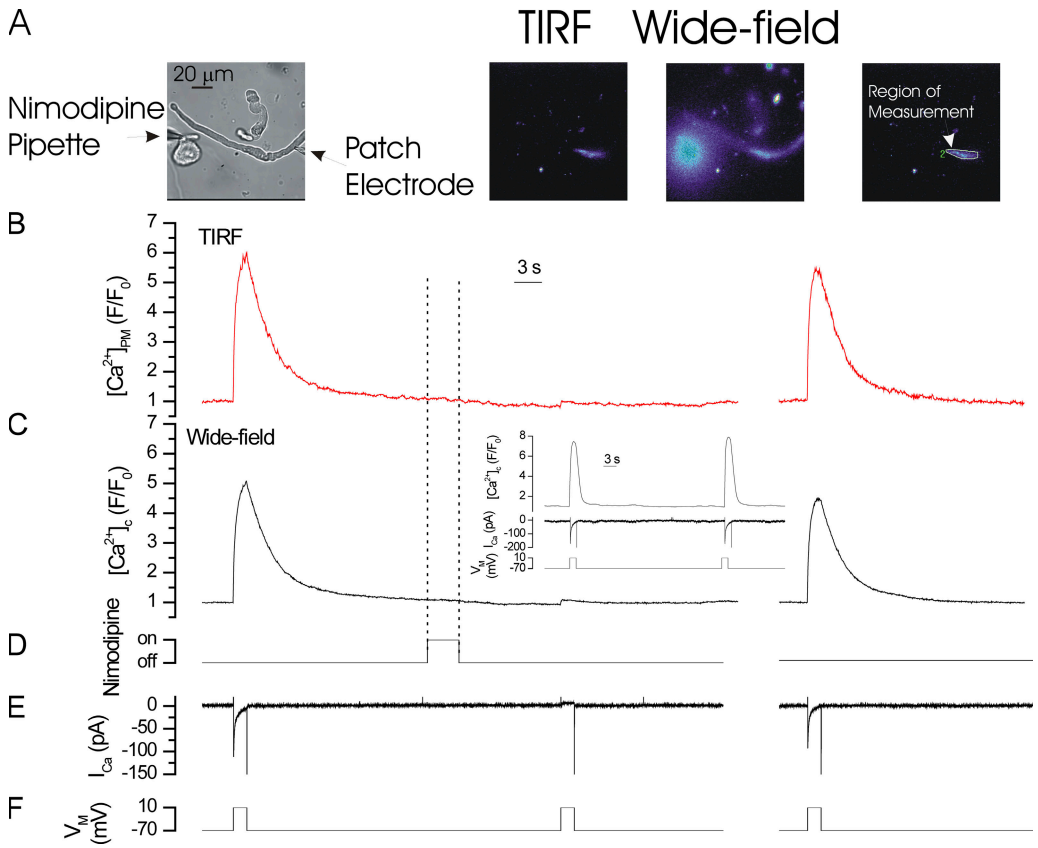

Figure 6. Nimodipine blocks I_{Ca} and accompanying $[Ca^{2+}]$ increase, but does not decrease resting $[Ca^{2+}]$ in voltage-clamped single colonic myocytes. Depolarization (−70 to +10 mV; F) activated a voltage-dependent Ca^{2+} current (I_{Ca}; E) to increase $[Ca^{2+}]$ in the subplasma membrane space (B) and bulk cytoplasm (C). Changes in the fluorescence ratio with time (B and C) are derived from the region encompassing that part of the cell in TIRF (A; right panel). 1 µM nimodipine (D) applied from a puffer pipette (A, left panel) did not alter resting subplasma membrane (B) or bulk average (C) $[Ca^{2+}]$ but blocked depolarization-evoked I_{Ca} (E) and the accompanying $[Ca^{2+}]$ rise (B and C). The break in the record is ∼3 min after which I_{Ca} and accompanying $[Ca^{2+}]$ increase partially recovered. A bright field image of the cell is shown in A (left panel); see also whole cell electrode (right side). The inset in C shows the bulk average $[Ca^{2+}]_c$ changes, which occurred in a cell using the same protocol except that nimodipine was not puffed onto the cell.

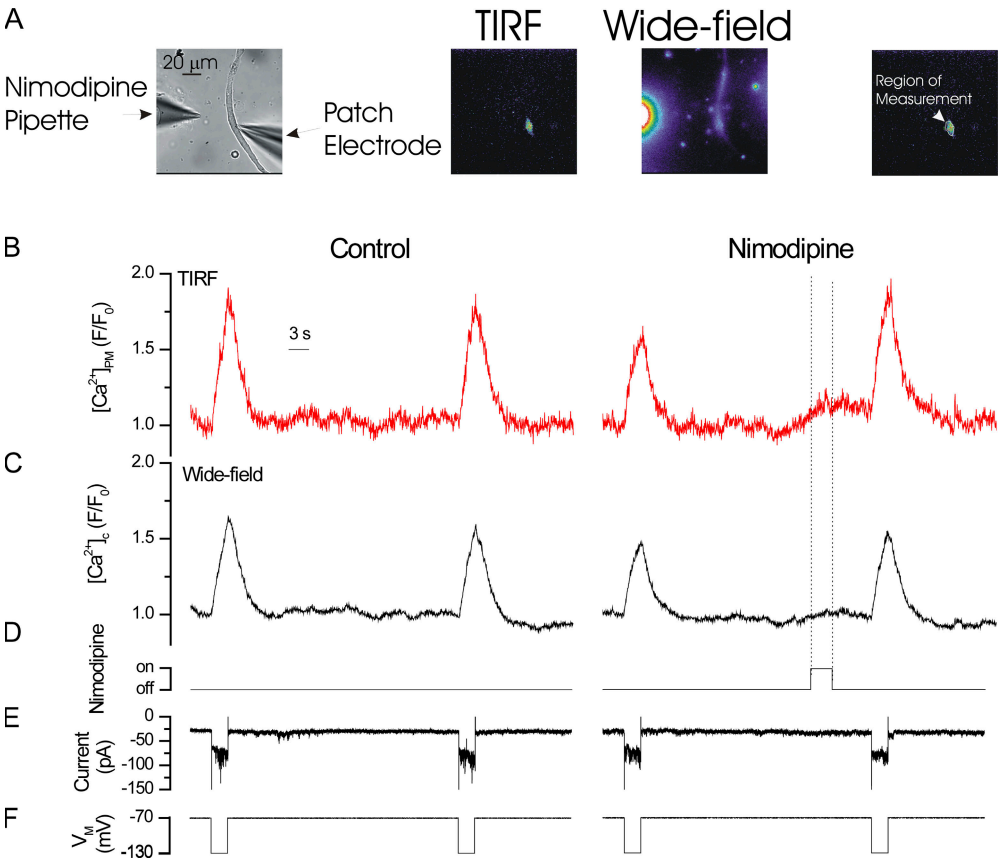

Figure 7. Nimodipine does not reduce the $[Ca^{2+}]$ increase evoked by hyperpolarization in voltage-clamped single colonic myocytes. Hyperpolarization (−130 mV; F) from the resting potential (−70 mV; F) increased $[Ca^{2+}]_{PM}$ (B) and $[Ca^{2+}]_c$ (C). The 60-mV hyperpolarization (to −130 mV) increases the electrochemical driving force on Ca^{2+} by an amount equivalent to a 100-fold increase in extracellular $[Ca^{2+}]$; i.e., an increase to 300 mM. In control (B–F, left panels), approximately reproducible rises were evoked by two hyperpolarizations separated by ∼60 s. In the next part of the experiment, the hyperpolarizations were repeated, but 1 µM nimodipine (D), an inhibitor of voltage-dependent Ca^{2+} channels, was applied by pressure ejection from a puffer pipette (D) before the second hyperpolarization. Nimodipine reduced neither the hyperpolarization-evoked $[Ca^{2+}]_c$ nor $[Ca^{2+}]_{PM}$ rise. The slight increase in $[Ca^{2+}]$ (B and C), which occurred just before nimodipine application (D), arose from a small change in holding current (E). (A; left panel) A bright field image of the cell; see also whole cell electrode (right side) and 1 µM nimodipine–containing puffer pipette (left side). Changes in the fluorescence ratio with time (B and C) are derived from the region encompassing that part of the cell in TIRF (A; right panel).

and accompanying $[Ca^{2+}]_c$ increases were blocked by nimodipine (Fig. 8 C). Thus, in control, depolarization-evoked (−70 to +10 mV) I_{Ca} averaged −157 ± 23 pA, its accompanying $[Ca^{2+}]$ rise in the bulk cytoplasm was 4.5 ± 1.1 ($\Delta F/F_0$), and in the subplasma membrane space it was 5.6 ± 1.5 ($\Delta F/F_0$; $n = 8$). After 1 µM nimodipine, I_{Ca} was −39 ± 13 pA ($n = 8$), its accompanying $[Ca^{2+}]$ rise in the bulk cytoplasm was 0.43 ± 0.15 ($\Delta F/F_0$), and in the subplasma membrane space it was 0.55 ± 0.17 ($\Delta F/F_0$; $n = 8$); each was significantly reduced ($P < 0.05$). After ∼3 min, I_{Ca} was −142 ± 22 pA, the $[Ca^{2+}]_c$ rise in the bulk cytoplasm was 5.9 ± 1.9 ($\Delta F/F_0$), and in the subplasma membrane space it was 7.4 ± 2.6 ($\Delta F/F_0$); each restored toward control levels ($n = 8$).

Nor did PKC activation with 10 µM indolactam-V alter the absence of effect of nimodipine on the $[Ca^{2+}]_c$ increase, which occurred on hyperpolarization (Fig. 8 D). Thus, hyperpolarization (−70 to −130 mV) evoked a $[Ca^{2+}]$ rise in the subplasma membrane space (0.29± 0.13 $\Delta F/F_0$; $n = 6$) and bulk cytoplasm (0.19 ± 0.06 $\Delta F/F_0$) (Fig. 8 D). After 1 µM nimodipine, the hyperpolarization-evoked $[Ca^{2+}]_c$ increase in the subplasma membrane space (0.38 ± 0.14 $\Delta F/F_0$; $n = 6$) and bulk cytoplasm (0.19 ± 0.06 $\Delta F/F_0$; $n = 6$) (Fig. 8 D) was unchanged when compared with control. Collectively, the channels that control bulk average $[Ca^{2+}]_c$ are not constitutively active dihydropyridine-sensitive Ca^{2+} channels.

Contribution of constitutively active channels to vascular smooth muscle $[Ca^{2+}]_c$ regulation

Perhaps constitutive activity is a feature of vascular rather than gastrointestinal smooth muscle (Navedo et al., 2005). However, in single smooth muscle cells from portal vein, although 1 µM nimodipine blocked I_{Ca} and the accompanying rise in $[Ca^{2+}]_c$, the drug did not reduce $[Ca^{2+}]_c$ at the resting membrane potential (−70 mV). Thus, before 1 µM nimodipine, resting bulk average $[Ca^{2+}]_c$ was 1.02 ± 0.04 (F/F_0), and after it was 1.04 ± 0.05 (F/F_0; $n = 6$; $P > 0.05$) (Fig. 9 A). Neither did resting $[Ca^{2+}]_{PM}$ change (1.25 ± 0.15 [F/F_0] before and 1.32 ± 0.18 [F/F_0; $n = 6$; $P > 0.05$] after 1 µM nimodipine). However, I_{Ca} and its accompanying $[Ca^{2+}]_c$ increase were blocked (Fig. 9 A). Thus, in control, depolarization-evoked (−70 to +10 mV) I_{Ca} averaged −84 ± 17 pA, and the accompanying $[Ca^{2+}]$ rise in the bulk cytoplasm was 1.98 ± 0.44 ($\Delta F/F_0$) and in the subplasma membrane space it was 2.1 ± 0.46 ($\Delta F/F_0$; $n = 6$). After 1 µM nimodipine, I_{Ca} (−5 ± 3 pA; $P < 0.01$) and the accompanying

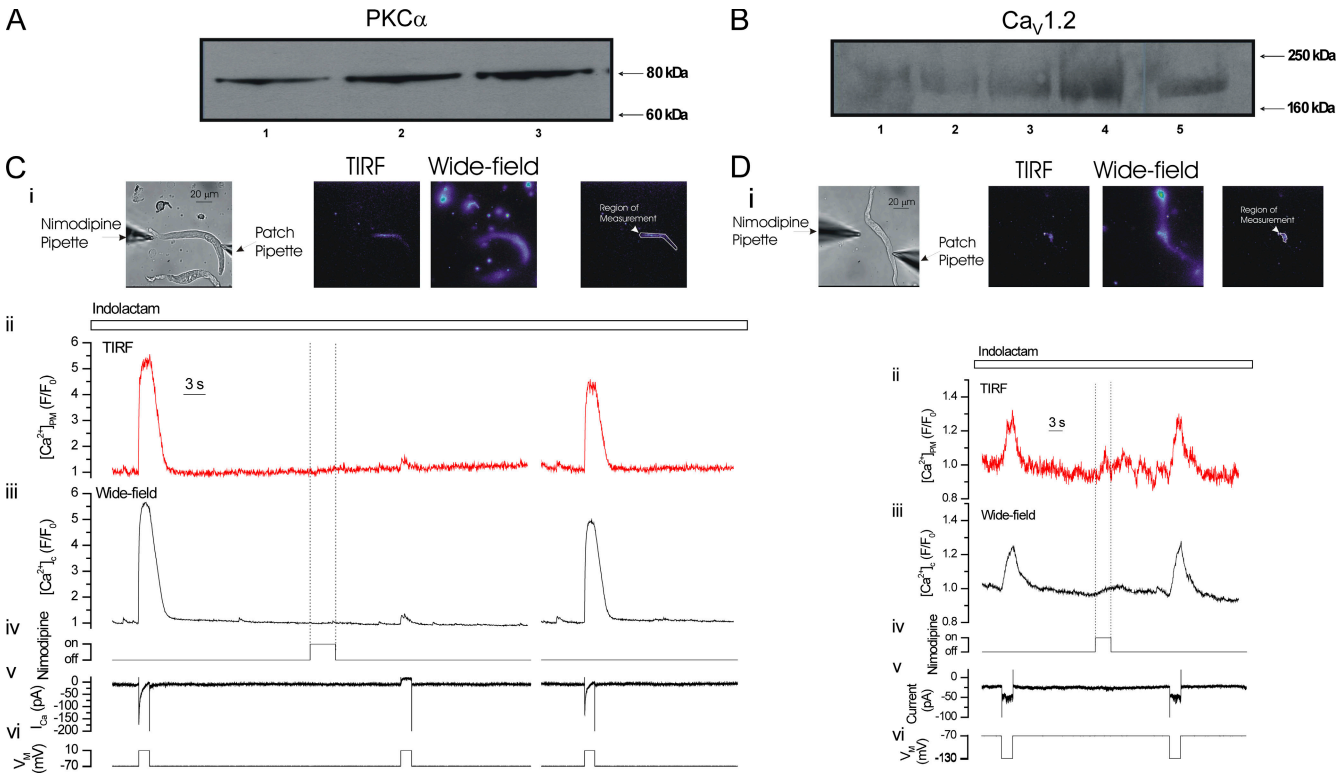

Figure 8. The PKC activator indolactam-V does not induce constitutive Ca^{2+} channel activity in colonic myocytes. (A) PKCα expression in colon. The immunoblot shows increasing loads of total protein (10, 15, and 20 μg in lanes 1–3) from guinea pig colon whole homogenate probed with mouse anti-PKCα monoclonal IgG1. The position of molecular weight markers, which were run alongside, is indicated. The result shown is typical of those obtained from two other independent experiments. (B) $Ca_V1.2$ expression in guinea pig colon. The immunoblot shows increasing loads of total protein (10, 20, 30, and 40 μg in lanes 1–4) from guinea pig colon whole homogenate probed with rabbit anti-$Ca_V1.2$ polyclonal antibody. Lane 5 shows cardiac ventricular homogenate (10 μg), which was used as a positive control for $Ca_V1.2$. The position of molecular weight markers run alongside is indicated. The result is typical of two other experiments. (C) In indolactam-V (a PKC activator; 10 μM; open bar above traces), depolarization (−70 to +10 mV; C, vi) activated a voltage-dependent Ca^{2+} current (I_{Ca}; v) to evoke a rise in $[Ca^{2+}]$ in the subplasma membrane space (ii) and bulk cytoplasm (iii). 1 μM nimodipine (iv) applied from a puffer pipette (C, i, left panel, Nimodipine Pipette) did not alter the subplasma membrane (ii) or bulk average (iii) $[Ca^{2+}]$, although it blocked depolarization-evoked I_{Ca} (v) and the accompanying $[Ca^{2+}]$ rise (ii and iii). The break in the record is ∼3 min after which I_{Ca} and $[Ca^{2+}]$ rise partially recovered. A bright field image of the cell is shown (C, i, left panel); see also whole cell electrode (right side). (D) Hyperpolarization (−130 mV; vi) from the resting potential (−70 mV; vi) evoked an increase in $[Ca^{2+}]_{PM}$ (ii) and $[Ca^{2+}]_c$ (iii). The PKC activator indolactam-V (10 μM; open bar) was present throughout. 1 μM nimodipine (iv), an inhibitor of voltage-dependent Ca^{2+} channels, was applied by pressure ejection from a puffer pipette (D, i, left panel) but did not reduce the hyperpolarization-evoked $[Ca^{2+}]_c$ rise. The small change in $[Ca^{2+}]$ (ii and iii) on nimodipine application (iv) occurred because of a slight change in the membrane current (v). Changes in the fluorescence ratio with time (C, ii and iii, and D, ii and iii) are derived from the regions encompassing that part of the cell in TIRF (C, i, and D, i, right-hand panels).

$[Ca^{2+}]$ rise in the bulk cytoplasm (0.05 ± 0.09 $\Delta F/F_0$; $P < 0.05$) and subplasma membrane space (0.03 ± 0.1 $\Delta F/F_0$; $n = 6$; $P < 0.05$) were each significantly reduced. After a further ∼3 min, I_{Ca} (−78 ± 11 pA) and the $[Ca^{2+}]_c$ rise in the bulk cytoplasm (0.88 ± 0.36 [$\Delta F/F_0$]) and subplasma membrane space (1.77 ± 0.44 [$\Delta F/F_0$]) were each restored toward control levels.

Next, in single portal vein myocytes, the effect of nimodipine on the Ca^{2+} entry evoked by an increased driving force on Ca^{2+} was examined (Fig. 9 B). Hyperpolarization (to −130 from −70 mV) evoked an increase in $[Ca^{2+}]_c$ (0.66 ± 0.12 $\Delta F/F_0$) and $[Ca^{2+}]_{PM}$ (0.81 ± 0.17 $\Delta F/F_0$; $n = 6$). 1 μM nimodipine blocked neither the hyperpolarization-evoked increase in $[Ca^{2+}]_c$ (0.71 ± 0.14 $\Delta F/F_0$; $n = 6$; $P > 0.05$) nor $[Ca^{2+}]_{PM}$ (0.95 ± 0.27 $\Delta F/F_0$; $n = 6$; $P > 0.05$) (Fig. 9 B). As a control, the presence of PKCα and $Ca_V1.2$ was confirmed (Fig. 9, C and D). These experiments suggest that constitutively active dihydropyridine-sensitive Ca^{2+} channels do not play a major role in regulating bulk average $[Ca^{2+}]_c$ in portal vein myocytes.

DISCUSSION

Ca^{2+} entry via dihydropyridine-sensitive Ca^{2+} channels is acknowledged to substantially determine bulk average $[Ca^{2+}]_c$ values in smooth muscle (Nelson et al., 1990; Sanders, 2008). However, the nature of the gating of the

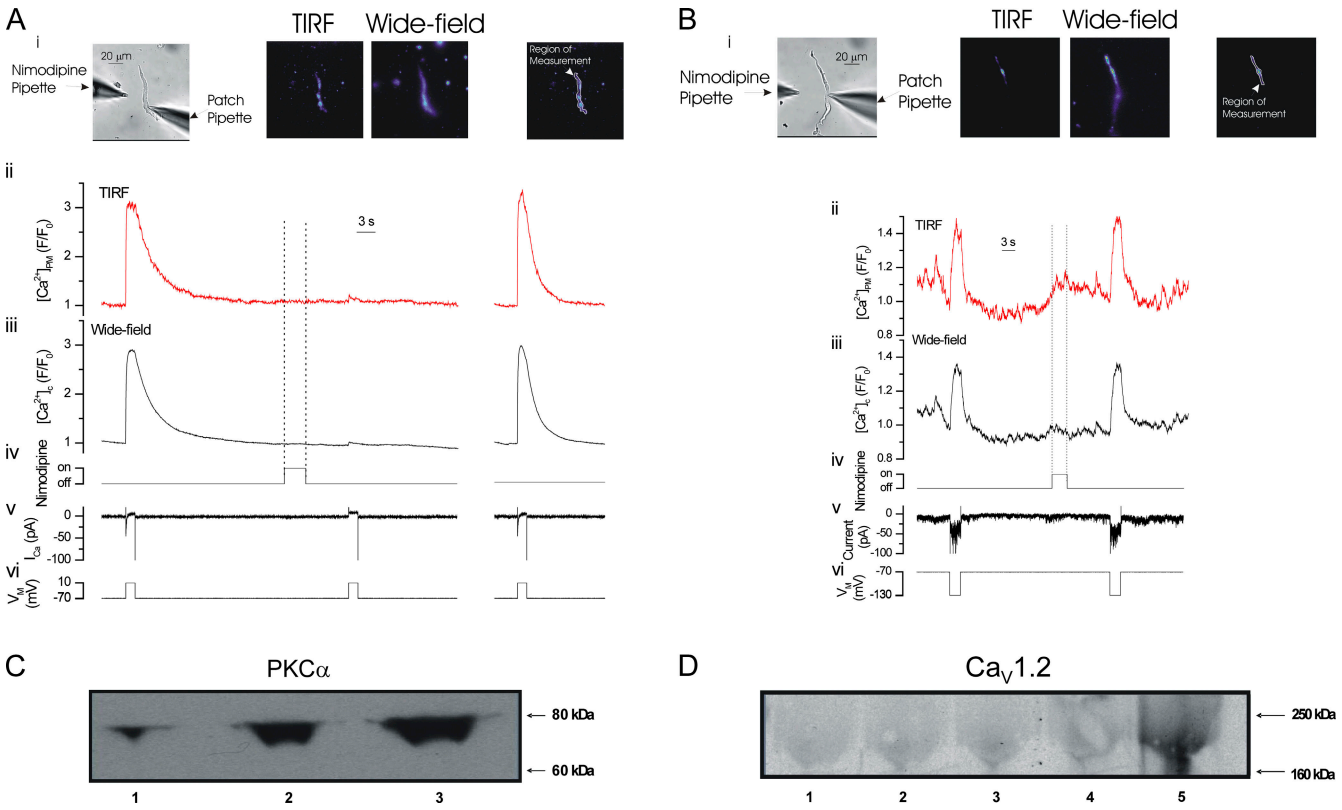

Figure 9. Lack of constitutive Ca^{2+} channel activity in vascular myocytes. (A) In single portal vein myocytes, depolarization (−70 to +10 mV; vi) activated a voltage-dependent Ca^{2+} current (I_{Ca}; v) to evoke a rise in $[Ca^{2+}]$ in the subplasma membrane space (ii) and bulk cytoplasm (iii). 1 µM nimodipine (iv) applied from a puffer pipette (A, i, left panel, Nimodipine Pipette) did not alter the resting subplasma membrane (ii) or bulk average (iii) $[Ca^{2+}]$ but blocked I_{Ca} (v) and the accompanying $[Ca^{2+}]$ rise (ii and iii). The break in the record is ∼3 min after which I_{Ca} and $[Ca^{2+}]$ partially recovered. A bright field image of the cell is shown (A, i, left panel); see also whole cell electrode (right side). (B) In single portal vein myocytes, hyperpolarization (−130 mV; vi) from the resting potential (−70 mV; vi) evoked an increase in $[Ca^{2+}]_{PM}$ (ii) and $[Ca^{2+}]_c$ (iii). 1 µM nimodipine (iv), an inhibitor of voltage-dependent Ca^{2+} channels, applied by pressure ejection from a puffer pipette (B, i, left panel) did not reduce the hyperpolarization-evoked $[Ca^{2+}]_c$ or $[Ca^{2+}]_{PM}$ rise. Changes in the fluorescence ratio with time (A, ii and iii, and B, ii and iii) are derived from the regions encompassing that part of the cell in TIRF (A, i, and B, i, right-hand panels). (C) PKCα expression in portal vein. The immunoblot shows increasing loads of total protein (10, 15, and 20 µg in lanes 1–3) from guinea pig portal vein whole homogenate, which was probed with mouse anti-PKCα monoclonal IgG1. The position of molecular weight markers run alongside is indicated. The result is typical of those obtained from two other independent experiments. (D) $Ca_V1.2$ expression in guinea pig portal vein. Immunoblot showing increasing loads of total protein (10, 20, 30, and 40 µg in lanes 1–4) from guinea pig portal vein whole homogenate, which was probed with rabbit anti-$Ca_V1.2$ polyclonal antibody. Lane 5 shows 10 µg cardiac ventricular homogenate used here as a positive control for $Ca_V1.2$. The position of molecular weight markers run alongside is indicated. Results shown are typical of two other experiments.

dihydropyridine-sensitive Ca^{2+} channel is disputed. In one proposal, the channel's gating is voltage dependent and stochastic (Rubart et al., 1996). In another, the channels are clustered, their gating coordinated, and they are constitutively active (Navedo et al., 2005). Here, the contribution of each form of activity to Ca^{2+} regulation has been studied in single colonic and portal vein myocytes. Wide-field epifluorescence and TIRF microscopy were combined to measure $[Ca^{2+}]$ near simultaneously in each of the bulk cytoplasm and subplasma membrane space. The results suggest that it is the stochastic voltage-dependent rather than constitutive activity of the channel that is significant in the control of $[Ca^{2+}]_c$.

Here, the depolarization-evoked $[Ca^{2+}]$ increase that occurred in bulk cytoplasm was approximately uniform in amplitude and time course, whereas that of the subplasma membrane space was not. Several localized rises in $[Ca^{2+}]_{PM}$ occurred in isolated regions of the subplasma membrane space, during depolarization, which had more rapid kinetics than the average. The localized changes are consistent with clustering of voltage-dependent Ca^{2+} channels in some regions of the plasma membrane. The activity of these clustered channels is regulated by membrane potential; the channels are largely closed at the resting potential, open on depolarization, and close when the depolarization ends. In other regions of the subplasma membrane space, increases in $[Ca^{2+}]_{PM}$ also occur, which are uniform in time course and amplitude. Thus, although there may be clustering of channels in some regions, there is also a

distribution of channels to generate a relatively uniform increase in the bulk of the subplasma membrane space.

Recently, clusters of constitutively active Ca^{2+} channels have been proposed to generate sites of near continual Ca^{2+} influx in 10% of that fraction of the plasma membrane that was imaged; i.e., presumably in excess of 20% of the total plasma membrane (Navedo et al., 2005). The constitutively active channels are suggested to determined the bulk average $[Ca^{2+}]_c$ (Navedo et al., 2005). In the present study, localized repetitive rises in $[Ca^{2+}]_{PM}$ (persistent Ca^{2+} sparklets), which are consistent with the activity of constitutively active L-type Ca^{2+} channels (Navedo et al., 2005, 2006; Amberg et al., 2007), were observed rarely (2 of 306 cells). Persistent Ca^{2+} sparklets appear to be an unusual behavior in the channels. Evidence for this conclusion is derived from an examination of the effects of a dihydropyridine inhibitor (nimodipine) of voltage-dependent Ca^{2+} channels over membrane potential ranges where channels that lack constitutive activity would be largely closed, but at which constitutively active channels would be expected to be open. At negative membrane potentials, voltage-dependent Ca^{2+} channels are largely closed. However, constitutive channel activity persists because PKCα acts like a 'switch' (Navedo et al., 2005, 2006; Amberg et al., 2007) to activate the channel regardless of membrane potential. The present results show that constitutive channel activity plays a minor role in the maintenance of bulk average $[Ca^{2+}]_c$. At the resting potential (−70 mV), rapid application of the inhibitor of voltage-dependent Ca^{2+} channels, which blocked I_{Ca} and accompanying $[Ca^{2+}]_c$ rise, neither reduced $[Ca^{2+}]_c$ nor $[Ca^{2+}]_{PM}$. The failure of the inhibitor of voltage-dependent Ca^{2+} channels to reduce $[Ca^{2+}]_c$ suggests that constitutively active channels contribute little to the resting $[Ca^{2+}]_c$. In another test of the contribution of constitutively active channels to determine bulk average $[Ca^{2+}]_c$, the membrane potential was hyperpolarized (−130 mV) from the resting value (−70 mV). The 60-mV hyperpolarization will increase the electrochemical driving force acting on Ca^{2+} by an amount equivalent to a 100-fold increase in extracellular $[Ca^{2+}]$; i.e., an increase in extracellular $[Ca^{2+}]$ to 300 mM. The inhibitor of voltage-dependent Ca^{2+} channels did not reduce the $[Ca^{2+}]_c$ increase that followed the hyperpolarization. Constitutively active Ca^{2+} channels seem unlikely to contribute substantially to the bulk average $[Ca^{2+}]_c$.

Constitutive channel activity requires PKCα and $Ca_V1.2$ (Navedo et al., 2005, 2006), each of which is in the smooth muscle types used in the present study. Activation of PKC using the phorbol ester–type tumor promoter indolactam-V did not induce constitutive channel activity at negative membrane potentials. In indolactam-V, neither bulk average $[Ca^{2+}]_c$ at −70 mV nor the increase that followed hyperpolarization to −130 mV was decreased by the inhibitor of voltage-dependent Ca^{2+} channels.

Although constitutively active channels contribute little at negative membrane potentials, their contribution is likely to diminish with depolarization. This situation arises because the open probability of the constitutively active channel is very high (0.18) at negative (−70 mV) membrane potentials and cannot increase further (Navedo et al., 2005, 2006). The electrochemical driving force on Ca^{2+} and unitary Ca^{2+} current amplitude each decrease substantially with depolarization, e.g., from −70 to −40 mV, the driving force for Ca^{2+} entry will decrease and unitary Ca^{2+} current amplitude will drop to ∼50% of its value at −70 mV (Rubart et al., 1996). Thus, if constitutively active channels play little role at negative (−70 mV) potentials, they would seem unlikely to contribute at depolarized (e.g., −40 mV) potentials unless additional clusters are recruited to constitutive activity.

In that respect, the spatial distribution of the Ca^{2+}-dependent PKCα isozyme rather than the distribution of the Ca^{2+} channel itself is of significance (Navedo et al., 2005, 2008). PKC may, it is proposed, recruit additional channels to constitutive activity. PKCα is localized to certain regions of the cell to phosphorylate the Ca^{2+} channel and evoke persistent channel opening at these sites regardless of membrane potential (Amberg et al., 2007). PKCα, a Ca^{2+}-dependent kinase, may be targeted to some regions of the plasma membrane (Navedo et al., 2008) but is generally thought to redistribute from an inactive "pool" in the cytoplasm to an active pool, such as the plasma membrane when it is itself activated by Ca^{2+} stimulation (Morgan and Leinweber, 1998). At "rest," little PKCα associates with the plasma membrane, and chelating Ca^{2+} using BAPTA prevents the translocation to the plasma membrane (e.g., Maasch et al., 2000; Nelson et al., 2008). Interestingly, persistent Ca^{2+} sparklets, the fluorescence manifestation of constitutive channel activity, were recorded using a high concentration (200 μM) of a Ca^{2+} indicator in cells that were dialyzed with even higher concentrations (10 mM) of the Ca^{2+} buffer EGTA (Navedo et al., 2005, 2006, 2007, 2008; Amberg et al., 2007). The buffering provided by EGTA would maintain the bulk cytoplasmic $[Ca^{2+}]_c$ at very low values (in the low picomolar range). How additional PKCα may be recruited to the plasma membrane to induce the formation of new clusters of channels with constitutive activity, e.g., by depolarization (Amberg et al., 2007), in the virtual absence of Ca^{2+} is unclear.

While persistent Ca^{2+} sparklets are proposed (Navedo et al., 2007) to be unaffected by nifedipine in cells that express mutant $Ca_V1.2$ channels resistant to dihydropyridines, the example traces (Fig. 6 A) (Navedo et al., 2007) in support of the proposal did not show persistent Ca^{2+} sparklets. Indeed, the conditions (presence of thapsigargin and EGTA) required to measure persistent Ca^{2+} sparklets (Navedo et al., 2005, 2006; Amberg et al., 2007) raise the possibility that channels other than the L-type voltage-dependent Ca^{2+} channel may contribute to the

$[Ca^{2+}]$ increase. The SR Ca^{2+} pump inhibitor (thapsigargin) and high concentration of EGTA (10 mM) are likely to deplete the SR Ca^{2+} store and activate store-operated Ca^{2+} entry. In resistance arteries (choroidal arteriolar smooth muscle; Curtis and Scholfield, 2001), store depletion by the SR Ca^{2+} pump inhibitor cyclopiazonic acid activated a store-operated Ca^{2+} current that was blocked by the same dihydropryidine antagonist (nifedipine) used to inhibit persistent Ca^{2+} sparklets. In an immature human monocytic cell line (U937 cells), store-activated Ca^{2+} entry, in response to store depletion by thapsigargin, was inhibited by nifedipine (Willmott et al., 1996). In murine erythroleukemia (MEL) cells, nifedipine blocked the Ca^{2+} entry evoked by a compound (hexamethylene bisacetaminde) that induced differentiation (Gillo et al., 1993). Pretreatment of MEL cells with Bay K8644 enhanced the effects of hexamethylene bisacetaminde (Gillo et al., 1993). MEL cells do not have a voltage-dependent Ca^{2+} current (Gillo et al., 1993), which again suggests that nifedipine may block other channels in addition to the voltage-dependent Ca^{2+} channel. Interestingly, although no voltage-dependent Ca^{2+} current existed, Northern blot analysis showed expression of mRNA that was homologous to the α_1 subunit of the cardiac L-type Ca^{2+} channel (Gillo et al., 1993). The implication is that the α_1 subunit may contribute to a channel with properties that are quite distinct from the L-type voltage-dependent Ca^{2+} channel in some cell types (Gillo et al., 1993).

In this study of voltage-dependent Ca^{2+} channel activity in gastrointestinal (colonic) and vascular (portal vein) smooth muscle, the L-type Ca^{2+} channel may be clustered in some regions of the plasma membrane to generate rapid rates of $[Ca^{2+}]$ change at these sites. The channel's voltage-dependent behavior appears sufficient to explain voltage-dependent Ca^{2+} entry and the rapid rates of $[Ca^{2+}]_{PM}$ change in some sites that may selectively target signals to effectors with rapid kinetics to allow specific cell functions to occur. The voltage-dependent Ca^{2+} channel in these tissues is not normally constitutively active; constitutive activity appears to contribute little to the regulation of $[Ca^{2+}]_c$. Although we have been unable to detect significant contributions from constitutively active Ca^{2+} channels in $[Ca^{2+}]_c$ regulation, it is possible that tissue (e.g., cerebral artery vs. portal vein and colon) or methodology (e.g., the lower external $[Ca^{2+}]$ in the present study) may contribute to the differences in results. The effects of inhibitors of voltage-dependent Ca^{2+} channels on bulk average $[Ca^{2+}]_c$ at negative membrane potentials (e.g., −70 mV) provides a straightforward test for the contribution of constitutively active channels in other tissues.

We are grateful to Dr Ernst Niggli for useful comments and suggestions.

This work was funded by the Wellcome Trust (078054/Z/05/Z) and British Heart Foundation (PG/06/016; PG/08/066), the support of which is gratefully acknowledged. A.J. Wright acknowledges support from the Royal Academy of Engineering/EPSRC.

Paul J. De Weer served as editor.

Submitted: 22 December 2008
Accepted: 25 February 2009

REFERENCES

Amberg, G.C., M.F. Navedo, M. Nieves-Cintron, J.D. Molkentin, and L.F. Santana. 2007. Calcium sparklets regulate local and global calcium in murine arterial smooth muscle. *J. Physiol.* 579:187–201.

Axelrod, D. 2001. Total internal reflection fluorescence microscopy in cell biology. *Traffic.* 2:764–774.

Bayguinov, O., S.M. Ward, J.L. Kenyon, and K.M. Sanders. 2007. Voltage-gated Ca^{2+} currents are necessary for slow-wave propagation in the canine gastric antrum. *Am. J. Physiol. Cell Physiol.* 293:C1645–C1659.

Beaumont, V. 2003. Visualizing membrane trafficking using total internal reflection fluorescence microscopy. *Biochem. Soc. Trans.* 31:819–823.

Bradley, K.N., J.W. Craig, T.C. Muir, and J.G. McCarron. 2004. The sarcoplasmic reticulum and sarcolemma together form a passive Ca^{2+} trap in colonic smooth muscle. *Cell Calcium.* 36:29–41.

Chalmers, S., and J.G. McCarron. 2008. The mitochondrial membrane potential and Ca^{2+} oscillations in smooth muscle. *J. Cell Sci.* 121:75–85.

Cohen, C.J., and R.T. McCarthy. 1987. Nimodipine block of calcium channels in rat anterior pituitary cells. *J. Physiol.* 387:195–225.

Currie, S., F.R. Quinn, R.A. Sayeed, A.M. Duncan, S. Kettlewell, and G.L. Smith. 2005. Selective down-regulation of sub-endocardial ryanodine receptor expression in a rabbit model of left ventricular dysfunction. *J. Mol. Cell. Cardiol.* 39:309–317.

Curtis, T.M., and C.N. Scholfield. 2001. Nifedipine blocks Ca^{2+} store refilling through a pathway not involving L-type Ca^{2+} channels in rabbit arteriolar smooth muscle. *J. Physiol.* 532:609–623.

Demuro, A., and I. Parker. 2004. Imaging the activity and localization of single voltage-gated Ca^{2+} channels by total internal reflection fluorescence microscopy. *Biophys. J.* 86:3250–3259.

Demuro, A., and I. Parker. 2005. "Optical patch-clamping": single-channel recording by imaging Ca^{2+} flux through individual muscle acetylcholine receptor channels. *J. Gen. Physiol.* 126:179–192.

Demuro, A., and I. Parker. 2006. Imaging single-channel calcium microdomains. *Cell Calcium.* 40:413–422.

Gillo, B., Y.S. Ma, and A.R. Marks. 1993. Calcium influx in induced differentiation of murine erythroleukemia cells. *Blood.* 81:783–792.

Gollasch, M., and M.T. Nelson. 1997. Voltage-dependent Ca^{2+} channels in arterial smooth muscle cells. *Kidney Blood Press. Res.* 20:355–371.

Maasch, C., S. Wagner, C. Lindschau, G. Alexander, K. Buchner, M. Gollasch, F.C. Luft, and H. Haller. 2000. Protein kinase C alpha targeting is regulated by temporal and spatial changes in intracellular free calcium concentration $[Ca^{2+}]_i$. *FASEB J.* 14:1653–1663.

MacMillan, D., S. Chalmers, T.C. Muir, and J.G. McCarron. 2005. IP_3-mediated Ca^{2+} increases do not involve the ryanodine receptor, but ryanodine receptor antagonists reduce IP_3-mediated Ca^{2+} increases in guinea-pig colonic smooth muscle cells. *J. Physiol.* 569:533–544.

McCarron, J.G., and T.C. Muir. 1999. Mitochondrial regulation of the cytosolic Ca^{2+} concentration and the $InsP_3$-sensitive Ca^{2+} store in guinea-pig colonic smooth muscle. *J. Physiol.* 516:149–161.

McCarron, J.G., D. MacMillan, K.N. Bradley, S. Chalmers, and T.C. Muir. 2004. Origin and mechanisms of Ca^{2+} waves in smooth muscle as revealed by localized photolysis of caged inositol 1,4,5-trisphosphate. *J. Biol. Chem.* 279:8417–8427.

McCarron, J.G., S. Chalmers, K.N. Bradley, D. Macmillan, and T.C. Muir. 2006. Ca^{2+} microdomains in smooth muscle. *Cell Calcium.* 40:461–493.

McCarron, J.G., S. Chalmers, and T.C. Muir. 2008. 'Quantal' Ca^{2+} release at the cytoplasmic aspect of the Ins(1,4,5)P_3R channel in smooth muscle. *J. Cell Sci.* 121:86–98.

McCarthy, R.T., and C.J. Cohen. 1989. Nimodipine block of calcium channels in rat vascular smooth muscle cell lines. Exceptionally high-affinity binding in A7r5 and A10 cells. *J. Gen. Physiol.* 94:669–692.

Morgan, K.G., and B.D. Leinweber. 1998. PKC-dependent signalling mechanisms in differentiated smooth muscle. *Acta Physiol. Scand.* 164:495–505.

Navedo, M.F., G.C. Amberg, V.S. Votaw, and L.F. Santana. 2005. Constitutively active L-type Ca^{2+} channels. *Proc. Natl. Acad. Sci. USA.* 102:11112–11117.

Navedo, M.F., G.C. Amberg, M. Nieves, J.D. Molkentin, and L.F. Santana. 2006. Mechanisms underlying heterogeneous Ca^{2+} sparklet activity in arterial smooth muscle. *J. Gen. Physiol.* 127:611–622.

Navedo, M.F., G.C. Amberg, R.E. Westenbroek, M.J. Sinnegger-Brauns, W.A. Catterall, J. Striessnig, and L.F. Santana. 2007. Ca(v)1.3 channels produce persistent calcium sparklets, but Ca(v)1.2 channels are responsible for sparklets in mouse arterial smooth muscle. *Am. J. Physiol. Heart Circ. Physiol.* 293:H1359–H1370.

Navedo, M.F., M. Nieves-Cintron, G.C. Amberg, C. Yuan, V.S. Votaw, W.J. Lederer, G.S. McKnight, and L.F. Santana. 2008. AKAP150 is required for stuttering persistent Ca^{2+} sparklets and angiotensin II-induced hypertension. *Circ. Res.* 102:e1–e11.

Nelson, C.P., J.M. Willets, N.W. Davies, R.A. Challiss, and N.B. Standen. 2008. Visualizing the temporal effects of vasoconstrictors on PKC translocation and Ca^{2+} signaling in single resistance arterial smooth muscle cells. *Am. J. Physiol. Cell Physiol.* 295:C1590–C1601.

Nelson, M.T., J.B. Patlak, J.F. Worley, and N.B. Standen. 1990. Calcium channels, potassium channels, and voltage dependence of arterial smooth muscle tone. *Am. J. Physiol.* 259:C3–C18.

Quayle, J.M., J.G. McCarron, J.R. Asbury, and M.T. Nelson. 1993. Single calcium channels in resistance-sized cerebral arteries from rats. *Am. J. Physiol.* 264:H470–H478.

Rizzuto, R., and T. Pozzan. 2006. Microdomains of intracellular Ca^{2+}: molecular determinants and functional consequences. *Physiol. Rev.* 86:369–408.

Roberts, W.M., R.A. Jacobs, and A.J. Hudspeth. 1990. Colocalization of ion channels involved in frequency selectivity and synaptic transmission at presynaptic active zones of hair cells. *J. Neurosci.* 10:3664–3684.

Rubart, M., J.B. Patlak, and M.T. Nelson. 1996. Ca^{2+} currents in cerebral artery smooth muscle cells of rat at physiological Ca^{2+} concentrations. *J. Gen. Physiol.* 107:459–472.

Sakmann, B., and E. Neher. 1995. Single-Channel Recording. 2nd Edition. Plenum Press, New York. 728 pp.

Sanders, K.M. 2008. Regulation of smooth muscle excitation and contraction. *Neurogastroenterol. Motil.* 20:39–53.

Vivaudou, M.B., L.H. Clapp, J.V. Walsh Jr., and J.J. Singer. 1988. Regulation of one type of Ca^{2+} current in smooth muscle cells by diacylglycerol and acetylcholine. *FASEB J.* 2:2497–2504.

Vivaudou, M.B., J.J. Singer, and J.V. Walsh Jr. 1991. Multiple types of Ca^{2+} channels in visceral smooth muscle cells. *Pflugers Arch.* 418:144–152.

Willmott, N.J., Q. Choudhury, and R.J. Flower. 1996. Functional importance of the dihydropyridine-sensitive, yet voltage-insensitive store-operated Ca^{2+} influx of U937 cells. *FEBS Lett.* 394:159–164.